運輸省港湾技術研究所

港湾技術研究所報告

REPORT OF THE PORT AND HARBOUR RESEARCH INSTITUTE MINISTRY OF TRANSPORT

VOL. 17 NO. 4 DEC. 1978

NAGASE, YOKOSUKA, JAPAN

港湾技術研究所報告　(REPORT OF P. H. R. I.)

第17巻　第4号 (Vol. 17, No. 4), 1978年12月 (Dec. 1978)

目　　次 (CONTENTS)

港湾技術研究所報告
第17巻 第4号 (1978. 12)

1. Random Wave Velocity Field From Periodic Theory

Koji Kobune*

Synopsis

Random waves are often expressed as a mathematical superposition of an infinite number of sinusodidal components. The mean square spectral density of the water surface elevation is often called the wave spectrum. The zero upcrossing wave heights usually have a Rayleigh probability distribution. However, the design wave concept is still used for design of many marine structures. It is common to use periodic wave theory to predict the velocity distribution in the design wave, even though it is known that actual waves are quite irregular and their shape and kinematics may not conform to the periodic theory.

The purpose of this study is to examine the validity of applying periodic wave theory to a wave in a random wave train. The magnitude of the errors are quantified in a statistical manner. The experiments were conducted in the Wave Research Facility at Oregon State University wherein random wave were generated with a flap-type wave board, resulting in a Bretschneider type spectrum with significant wave heights from 60 to 85 cm and significant periods from 2.5 to 2.8 secs. The water particle velocities were measured with a hot film anemometer and a propeller current meter.

The observed maximum horizontal and vertical velocities of each zero upcrossing wave were compared with predicted ones from the linear wave theory. The relative error is expressed as

$$r=\frac{u_{\text{measured}}-u_{\text{Predicted}}}{u_{\text{predicted}}}.$$

The relative error turned out to be normally distributed and the standard deviation varied from 0.1 to 0.6 according to the size of the wave sample, although the mean value of the error remained almost constant. The error was smallest for the large waves which gives confidence to the use of periodic theories for the design wave concept even though random waves are experienced by the structure.

* Chief of Storm Surge and Tsunami Laboratory, Hydraulic Engineering Division

REPORT OF THE PORT AND
HARBOUR RESEARCH INSTITUTE
Vol. 17, No. 4 (Dec. 1978)

1　規則波理論による不規則波中の水粒子速度の算定

小　舟　浩　治*

要　旨

不規則な海の波の数学的表示法として，周波数の異なる多数の正弦波を重ね合わせることにより表わす，いわゆるスペクトルによる表示法がある。

しかし，多くの港湾構造物の設計では，不規則波群中の代表波（設計波）を，その波高および周期が等しい規則波と見なし，規則波理論あるいは規則波実験に基づく検討結果を用いて波の作用状況を解析する，という方法が広く用いられている。ところが不規則な波形を持つ設計波に対し，規則波理論を適用することの妥当性について，これまでに詳細に検討されたことはなく，単に便宜的に用いているのが現状である。

本研究は，こうした不規則波に対する規則波理論の適用性検討の一つとして，規則波理論により不規則波中の水粒子速度を算定した場合に生じる誤差について考察したものである。

実験は長さ 104m，幅 3.7m，水深 3.75m の水路で行ない，水粒子速度をプロペラ式流速計およびホット・フィルム流速計により測定した。水粒子速度の測定値および算定値を比較検討した結果，次式で与えられる相対誤差との分布は正規分布であり，不規則波中の大きい波群における相対誤差の標準偏差は，小さい波群のそれよりも小さいことがわかった。

$$r=\frac{u_{\text{measured}}-u_{\text{predicted}}}{u_{\text{predicted}}}$$

このことは，設計対象となる大きい波については，規則波理論により比較的正確な水粒子速度の算定が可能であることを示している。

*　水工部　高潮津波研究室長

Table of Contents

1 Introduction

Two different methods have been developed to represent random ocean waves for the prediction of wave forces on marine facilities. One is a conventional method which uses the design wave concept designated by a height ($\bar{H}_D$) and period (T_D) and direction. The other utilizes the mean square spectral density of the water surface fluctuation which is often called the wave spectrum.

The latter method has become of interest for the dynamic analysis within the design of marine structures, such as offshore oil facilities. These structures are less stiff in comparison with massive structures such as sea walls and breakwaters, and their stability should be examined against the continuous random wave action. Thus, many studies on random wave-structure dynamic interaction have been made, and the validity of this analysis is being confirmed.

On the other hand, the design of many other marine facilities are still dependent on the first method. These structures are stiff and can be designed to resist waves by means of a static analysis.

In the process of the design wave method, a design wave is chosen to represent a severe sea condition for the structure in a depth of water, h. The design wave is characterized by its height, H_D, and its period, T_D, which are determined on the basis of a statistical study, wave records, hindcasting, experience and judgement. The design wave height is usually a large, rare value, and sometimes can be specified as some factor (e. g. 2. 0) times the significant weve height (the average of the 1/3 highest waves).

The water kinematics within thus chosen design wave are estimated by fitting a periodic wave to the design wave and utilizing an appropriate periodic wave theory. However, the design wave as it occurs in nature may have an irregular profile rather than a smooth profile as given by the wave theory.

The purpose of this study is to examine the validity of the design wave method by estimating the magnitude of error to be expected when periodic wave theories are used to predict the kinematics within random waves.

Random waves were generated in the Wave Research Facility at Oregon State University. Discrete zero upcrossing waves were selected to compare the predicted water particle velocities from a periodic wave theory with the measured ones. The results show that the periodic wave theory do adequately predict water particle velocities for the large waves. This is fortunate because the design wave method is used with the large waves.

2 Literature survey

2.1 Velocity measurements in random waves

Studies of random waves concerning wave forces have been conducted from increasing requests for the construction of submarine pipe lines and large pile supported marine structures. In these studies, the dynamic structure responses, such as bending moment imposed on the structure members and deflection of a whole structure, are of principal interest. Thus, many efforts have been made to develop mathematical models of wave-structure interaction on the basis of linear superposition of sinusoidal waves: R. O. Reid [1], L. E. Borgman[2], J. H. Nath and D. R. F. Harlemean[3]. The availability of these mathematical models to predict the kinematics of random waves can not be confirmed until they are examined through velocity and acceleration measurements.

Y. Iwagaki et. al.[4] measured water particle velocities of random waves utilizing a sonic doppler current meter. They found that Reid's numerical filter[5] given by Eqs. (2. 1) and (2. 2) provided a fairly good estimate of the time variation of wave kinematics, given the time series of the water surface elevation $\eta(t)$.

$$u(t)=a_0\eta(t)+\sum_{m=1}^{N}a_m[\eta(t+m\tau)+\eta(t-m\tau)] \tag{2.1}$$

$$w(t)=\sum_{m=1}^{N} b_m[\eta(t+m\tau)-\eta(t-m\tau)], \tag{2.2}$$

where a_m and b_m are Fourier coefficients in the Fourier expansion of the frequency response functions. That is,

$$a_m=\frac{1}{\pi}\int_0^{\omega_s\tau} R_u(\omega)\ \cos\ m(\omega\tau)\ d(\omega\tau),\quad m=0,1,2\ldots,N \tag{2.3}$$

$$b_m=\frac{1}{\pi}\int_0^{\omega_s\tau} R_w\ (\omega)\ \sin\ m(\omega\tau)\ d(\omega\tau),\quad m=1,2,3\ldots,N \tag{2.4}$$

where ω_s is the cut-off frequency, and

$$R_u(\omega)=\frac{\omega\ \cosh\ k(h+z)}{\sinh\ kh} \tag{2.5}$$

$$R_w(\omega)=\frac{\omega\ \sinh\ k(h+z)}{\sinh\ kh} \tag{2.6}$$

and k is the wave number, $2\pi/L$, with L the wave length.

Figure 2.1 shows the comparison of the velocity variation with the water surface elevation of their experiment. It is seen that the horizontal velocity variation closely followed the water surface elevation and its maxima and minima appear at the wave crests and troughs respectively. In addition, the vertical velocity is related to the slope of water surface and the peaks appear when the water surface crosses the still water level. Thus, discrete waves in a random wave train have similar general characteristics to periodic waves.

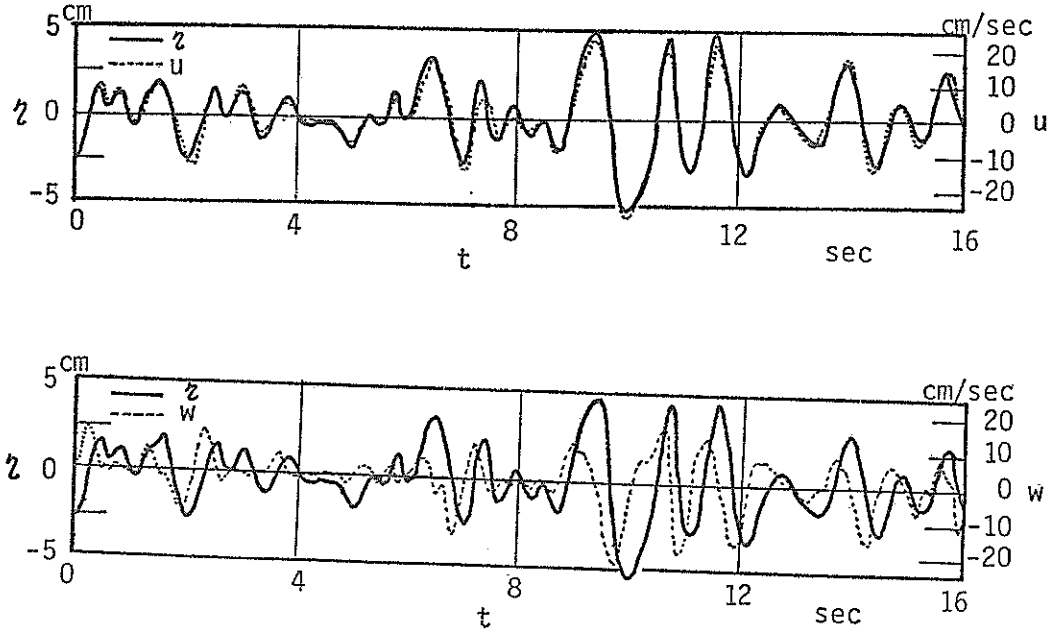

Fig. 2.1 Measured surface elevation and velocities of random wave (after Iwagaki, Sakai and Ishida, 1973)

In addition to the time variation of velocities, the frequency response function was discussed[4]. The measured response function, which was defined as Eqs. (2.7) and (2.8), turned out to be larger than the response function given by Airy theory, Eqs. (2.5) and (2.6), for the higher frequency range.

$$[R_u(\omega)]_{measured}=\sqrt{\frac{S_{uu}(\omega)}{S_{\eta\eta}(\omega)}} \tag{2.7}$$

$$[R_w(\omega)]_{measuerd}=\sqrt{\frac{S_{ww}(\omega)}{S_{\eta\eta}(\omega)}} \tag{2.8}$$

Where $S_{\eta\eta}(\omega)$, $S_{uu}(\omega)$ and $S_{ww}(\omega)$ are the power spectral density of water surface elevation, horizontal velocity and vertical velocity, respectively.

They commented that such a difference was partly caused by the noise of the current meter.

Y. Tsuchiya and Yamaguchi[6] measured the velocity of wind generated waves in a recirculation wave tank utilizing the sonic doppler current meter. The results of their measeurets yielded similar conclusions to Iwagaki's study because of contamination of the records with noise from the current meter.

Apart from the spectrum analysis, the discussion about the water particle velocities of discrete waves in a random wave train is seen in the study by R. A. Grace and R. Y. Rochelean[7]. They measured the near bottom velocities beneath the wave crests and troughs of long period waves (from 14 to 20 seconds) at the Waikiki shore, Hawaii, utilizing a propeller currrent meter. For this wave period range and water depth (10. 6m), Airy theory gives an almost constant ratio of the horizontal velocity beneath a wave crest, u_+, to the wave height, H. That is

$$u_+/H=0.476. \tag{2.9}$$

The wave height H_p, was calculated with Airy wave theory from the pressure measured at the bottom. The field work showed that the velocity, u_+, was linearly related to the wave height H_p just like the relation given by Airy thoery, Eq. (2.9), and that the leat-squares method yielded the following linear regression relation.

$$u_+/H_p=0.544 \tag{2.10}$$

where the wave height, H_p, was defined as the average of the trough to crest height fore and aft the crest. Thus, their definition is different from the zero upcrossing wave height.

The residuals which exist between the measured velocity and the velocity calculated from Eq. (2. 10) were examined. The distribution of the residuals turned out to be normal with the mean of -0.183cm/s and the standard deviation of 7. 254 cm/s.

As mentioned above, the wave heights used in their comparison were calculated from the measured pressure. These calculated wave heights are usually smaller than true (surface) wave heights[8]. This may have caused the difference between the coefficients in Eq. (2. 9) and Eq. (2. 10). The authors introduced a correction factor n_c, so that the true wave heights were estimated by Eq (2. 11).

$$H=n_cH_p \tag{2.11}$$

From Eqs. (2. 9) and (2. 10), the correction factor is calculated as

$$n_c=1.15. \tag{2.13}$$

This value is consistent with the value listed by Grace[8].

From the above discussion, the authors concluded that Airy theory peovided an excellent prediction of the mean realization of the velocity beneach the wave crests. This can be expressed by the following equation.

$$\frac{1}{N}\sum_{i=1}^{N}[u_+]_{\text{precicted by Airy theory}}=\frac{1}{N}\sum_{i=1}^{N}[u_+]_{\text{measured}} \tag{2.13}$$

2.2 Velocity measurement equipment

Accurate measurements of the water particle velocities in wave motion are difficult to make, and a variety of equipment has been used.

2.2.1 Propeller current meter

Propeller current meters are common instruments to measure quasi steady flows such as wind, open channel flow. flow in ducts, tidal flow and so on. However there is a difficulty in using them in waves, especially in laboratory wave tanks, because of usual low dynamic response to high frequency

fluctuation. In addition, they are usually not very sensitive to low speed steady flow.

Y, Goda[10] overcame the difficulty by utilizing small propellers (diameters of 3.5cm) and a large wave tank (water depth: from 1m to 2m, wave height: from 15cm to 80cm and wave period: from 2s to 8s). Based on the experiments, he proposed the following empirical formula to estimate the horizontal velocity beneath the wave crests.

$$u_+=\sqrt{1+\alpha\left(\frac{H}{h}\right)^{1/2}\left(\frac{s}{h}\right)^3}\cdot\frac{\pi H}{T}\frac{\cosh ks}{\sinh kh} \tag{2.14}$$

where α is a coefficient which varies from 1.5 to 0.25 depending on the ratio of the water depth to the wave length h/L_A, H is the wave height, T is the wave period, L_A is the wave length given by Airy theory, $k=2\pi/L_A$ and s is the distance from the bottom. Goda gave the coefficients, α, for various conditions as shown in **Table 2.1.**

Table. 2.1 Velocity factor α

h/L_A	0.03	0.05	0.07	0.10	0.14	0.20	0.30	0.50	0.70
α	1.50	1.50	1.43	1.25	0.97	0.68	0.49	0.25	0.27

Equation (2.14) modifies the horizontal velocity given by Airy theory in order to correctly express the large velocity near the still water level. According to the comparison among the available theories done by Dean[10], Eq. (2.14) gives as good fit with measured velocities as Dean's Stream Function Theory. Hence, Dean's Stream Function Theory gives good estimates of the horizontal velocity beneath the wave crests.

2.2.2 Photographic method

The water particle motion can be visualized with tracers, such as neutrally buoyant particles and/or hydrogen bubbles. Thus, the particle velocities in waves can be measured with the aid of a high speed movie camera. This method is suitable for experiments in small wave tanks. Measurements from this method have provided much information of the kinematics of finite amplitude waves: LeMehaute[11], Dean[12] and Iwagaki[13].

2.2.3 Hot film anemometer

Hot film and hot wire anemometers are common instruments for the measurement of turbulence in air flows. They have been improved so that they can be operated in water as well as in the air. Their characteristics in water have been examined by many researchers, some of whom are Richardson and McQuivey[14], Morrow and Kline[15] and Kato and Sano[16].

However, besides the usual difficulties in the operation of hot flm anemometrs, such as zero velocity drift due to fluid temperature change and the accumulation of dirty materials on the sensor, there are some inconveniences when they are used for velocity measurements in waves. A hot film sensor is sensitive to the magnitude of a flow speed and it can not detect the flow direction when the velocity vector is in the plane perpendicular to the hot film axis, Another is the strong non-linearity in the correlation between the flow speed and the output voltage when the flow speed varies over a wide range. In addition, the film is sensitive to the flows of which direction is parallel to the film axis.

Y. Iwagaki and T. Sakai[13] used a pair of hot film anemometers to measure the water particle velocity near the bottom, where the vertical velocity component vanishes and the output voltage corresponds to the magnitude of the horizontel veiocity. They operated two probes simultaneously: one is used to measure the velocity during the passage of wave crests and the other masured during the passage of wave troughs. The records from these two probes were connected at the times when the voltages of these two are equal.

The results show that measured velocity variations were similar to Stokes third order theory[17] for intermediate water condition and Hyperbolic waves[18] for shallow water conditions.

Some methods to measure water particle velocities in the upper region rather than near the bottom region have been developed by Kolpak and Eagleson[19] and Van Dornand Pazan[20]. The former used

a small direction vane to detect the flow direction, and compared the results with those measured by photogoraphic methods. They found the resulting directional error to be small enough when the ratio of the vane width to the radius of curvature of the water particle orbit was less than 0. 1, In addition, they cautioned that high sensor operating temperature might cause contamination of the record due to heated wakes for a stationary probe. Van Dorn used an orthogonal pair of wedge type hot film probes and measured the velocity distribution at the crests of near breaking waves. The procedure to obtain the magnitude and the direction of the flow is complicated. The principle can be summerized as follows.

Suppose the orthogonal pair of the hot film probes are installed as shown in **Fig. 2. 2.** and the range of θ is limited within the range from $-\pi/4$ to $\pi/4$. The non-linear output voltages from these probes have the following relation with the magnitude of the flow speed, V, and the direction, θ.

$$(E_B^2-E_O^2)_1=V^n\ \alpha_1(\theta_1)=V^n\ \alpha_1(\frac{\pi}{4}+\theta) \tag{2.15}$$

$$(E_B^2-E_O^2)_2=V^n\ \alpha_2(\theta_2)=V^n\ \alpha_2(\frac{\pi}{4}-\theta) \tag{2.16}$$

where E_B is the non-linear output voltage, E_O is the zero flow output voltage, n is a coefficient, $\alpha(\theta)$ is a directional coefficient and the suffix 1 and 2 show the variables are concerning Probe 1 and Probe 2, respectively. The coefficients n and $\alpha(\theta)$ and the zero flow output voltage E_O are determined through calibrations.

From Eqs. (2. 15) and (2. 16), the following equations are obtained.

$$\frac{(E_B^2-E_O^2)_1}{(E_B^2-E_O^2)_2}=\frac{\alpha_1(\frac{\pi}{4}+\theta)}{\alpha_2(\frac{\pi}{4}-\theta)}$$

For the measured ratio $(E_B^2-E_O^2)_1/(E_B^2-E_O^2)_2$, the flow direction θ can be found from a table of $\alpha_1(\frac{\pi}{4}+\theta)/\alpha_2(\frac{\pi}{4}-\theta)$.

Having found θ, the corresponding flow speed V is calculaied by either equation Eq. (2. 15) or Eq. (2. 16).

2. 2. 4 Ultra sonic doppler current meter and laser doppler anemometer

As mentioned in **Section 2. 1** and shown in **Fig 2. 1**, ultra sonic doppler current meters have been used to measure the velocities in random waves, and have brought fruitful results. This currenter can be operated not only in laboratory wave tanks but also in the ocean as described by Tsuchiya and Yamaguchi[16].

Recently the laser doppler anemometers have been developed. Lee, Grated and Durrani[21] tested this anemometer in periodic and random waves. They reported that it was a highly suitable instrument for laboratory study of waves. A full discussion about the kinematics of random waves, however, is not given in this papper.

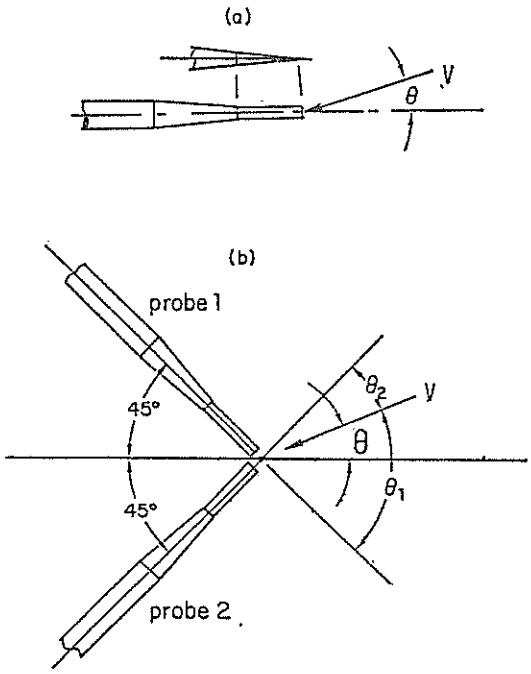

Fig. 2. 2 : (a) single, and (b) orthogonal hot film probe geometry. (after Van Dorn, 1975)

3 Facilities and equipment

3.1 Wave tank and wave generator

All the experiments were conducted in the Wave Research Facility at Oregon State University. The wave tank is 104m long, 3.7m wide and 4.6m deep except near the wave board, where the bottom of the tank is three feet deeper than the main part. The wave absorber is a concrete beach with a slope of one on twelve. The reflection coefficient of this beach is reported to be from 2.8% to 11.8% for the wave periods ranging from 0.95 seconds to 5.06 seconds[22]. **Figure. 3.1** shows the general view of the wave tank.

The wave generator is in the deepr end of the tank and has a flap type wave board. The wave board is driven by a hydraulic piston which is controlled by a potentiometric hydraulic servo system. The servo system is activated by an electric input, which can be either sinusoidal or random signal.

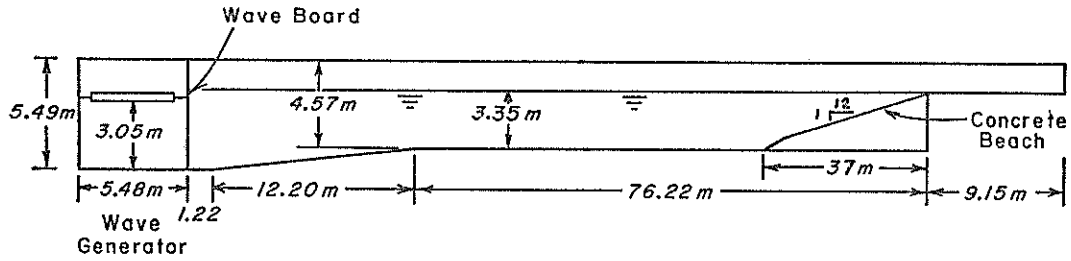

Fig. 3.1 : General view of wave tank

3.2 Measurement of water surface elevation

The water surface elevations for this work were measured with a Sonic System Model 86 Sonic Wave Profiler. The system operates by measuring the travel time required for a sound pulse to propagate from the sound source (a spark) to the water surface and return to the microphone. A signal conditioner converts the travel time to distance and from this the oscillating water surface is defined.

3.3 Measurements of velocity

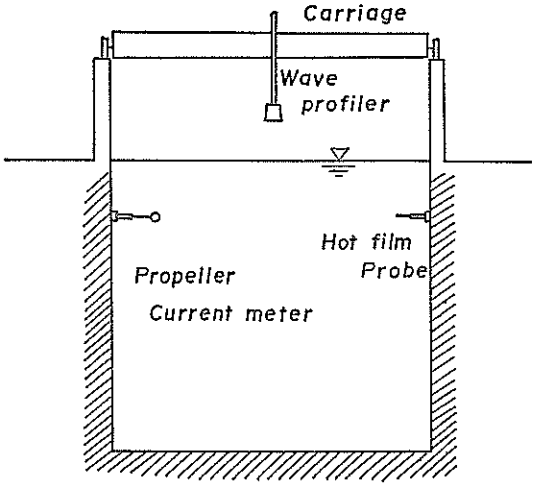

Fig. 3.2 : Probe set up (looking from the wave board)

Photo 3.1 : Propeller probe

The water particle velocities were measured utilizing two kinds of instruments: 1) a Nover Nixon Streamflo probe 403 propeller current meter, and 2) a Thermo System Inc. (TSI) 1240-60w X-type cylindrical hot film probe coupled with TSI Model 1050 constant temperature anemometers and Model 1052 Linearizers. These two probes were installed on the side walls of the wave tank (see **Fig. 3. 2**).

3. 3. 1 Nover Nixon Streamflo propeller probe (**Photo 3. 1**)

The propeller of the probe has a diameter of 1. 2cm as shown in **Fig. 3. 3.** It is composed of five blades mounted on a hard stainless steel spindle. Both ends of the spindle are fine burnished conical pivots which run in jewels in a frame. An insulated gold wire tip contained in the head of the slim tube, which supports the frame, terminates 0. 1 mm from the blade tips. When the propller revolves by the movement of a liquid past the blades, the passage of a blade past the gold wire tip slightly varies the measurable impedance between the tip and the tube. The variation of the impedance is amplified and it generates an electric pulse.

The calibration of the propeller probe (see **Appendix A**) shows that the inertia and the friction of the propeller is small and the propeller can trace an alternating flow of 3. 0 seconds period. In addition, the propeller is sensitive only to the velocity component which is parallel to the propeller spindle. Probe has a good dynamic response to the wave motion with a period longer than 3. 0 seconds. Though the response of the propeller to an alternating flow with shorter period than 3. 0 seconds is not tested through calibration, it will be examined through the comparison of the results from the propeller current meter with the measured velocity with the hot film anemometer in the periodic wave (**Section 4. 1**).

3. 3. 2 TSI hot film probe (**Photo 3. 2**)

The hot film probe has an orthogonal pair of quartz coated cylindrical hot film sensors with diameters of 0. 15 mm and sensing lengths of 2. 0 mm. The space between the sensors is 1. 0 mm. The probe was operated at low overheating ratio (1. 03) throughout the experiments in order to avoid the generation fo air bubbls on the sensor surface.

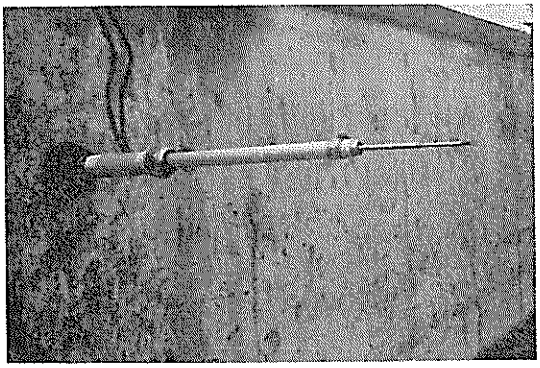

Photo 3. 2 : Hot film probe

The hot film anemometer output is an analog voltage, E_B, functionally realated to the flow speed, V, past the sensor as Eq. (2. 15) or Eq. (2. 16), For convenience in data processing, the output voltage, E_B, is linearized utilizing a TSI Model 1052 Linearizer. The linearizer approximates the non-linear relation between E_B and V by the following fourth order polynomial.

$$E=\sum_{i=1}^{4} C_i (E_B - E_0)^i \tag{3. 1}$$

where E is the linearized output voltage and C_i's are the coefficients to be determined through calibrations.

Thus, the relation of the linearized output voltage to the flow speed is expressed as follows.

$$E=A(\theta)\,V \tag{3. 2}$$

where $A(\theta)$ is the directional coefficint for the linearized output voltage. The directional coefficient, $A(\theta)$, takes a maximum when the yaw angle, θ, is zero and decrease according to the increase of θ, up to 90 degree, but it is not a cosine function. This shows that the linearized output voltage does not give a true normal velocity component to the sensor axis unless θ is zero. As mentioned in **Chapter 4**, it is possible to redue the horizontal and vertical velocity from the records obtained by simultaneous operation of an orthogonal pair of sensors if the directional coefficient $A(\theta)$ is determined correctly[13]. However, because the main purpose of this experiment is to measure the maximum and

centimeter

minimum magnitude of the horizontal and vertical velocity components, the complete analysis of the velocity components is not done for this study.

The probe was installed so that Sensor 1 (outer sensor) was vertical and Sensor 2 (inner sensor) was horizontal. Thus, the former was most sensitive to the horizontal velocity component while the latter was most sensitive to the vertical velocity component. In the data reduction, the maximum values among the analog output voltage were processed using the calibration curve for $\theta=0°$.

The hot film probe and the support are shown in **Fig. 3.4**, and the sensor orientation is shown in **Fig. 3.5**. The calibration procedures and the results are described in detail in **Appendix A.**

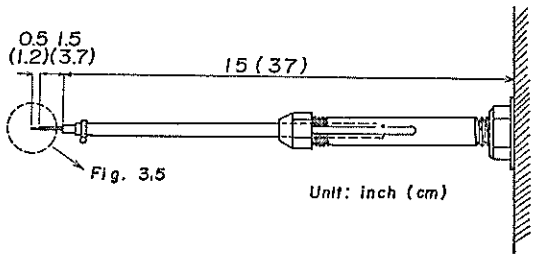

Fig. 3.4 : Hot film probe and support

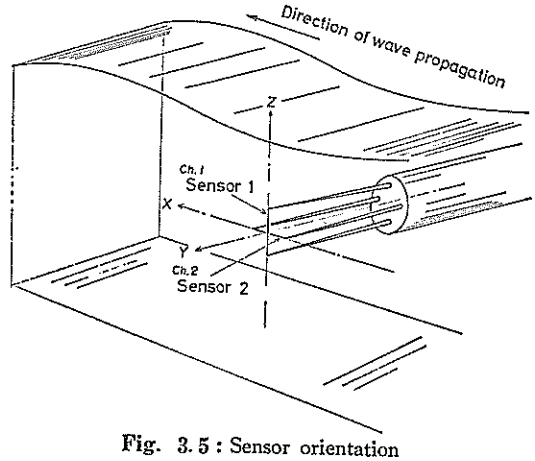

Fig. 3.5 : Sensor orientation

4 Results of experiments

4.1 Periodic waves

4.1.1 Wave conditions

Periodic wave tests were conducted with the aim to examine the accuracy of Airy theory with the hot film anemometer when it is used to measure the horizontal and vertical velocity components. Both the hot film anemometer and the propeller current meter were operated simultaneously.

The wave conditions are listed in **Table 4.1**. These conditions reflect those listed in the reference[24] and cover a wide range of wave periods and wave heights within the capacity of the wave generator. The water depth, h, was 3.35m throughout the experiments.

4.1.2 Sample record

A sample of the records is shown in **Photo 4.1**. Those records are, from the top, water surface elevation, non-linear output from the hot film anemometer channel 1 (Sensor 1), non-linear output from channel 2 (Sensor 2), linearized output from channel 1, linearized output from channel 2 and the output from the propeller current meter.

(1) Propeller current meter

It is obviously seen that the pulses are dense at a wave crest and trough. The maximum freqency, n, of the pulses was determined as the mean frequency over a period from 0.2 to 0.3 seconds under the wave crest and the wave trough. The maximum velocities were reduced by following relation obtained from the calibration (**Appendix A**).

$$u \text{ or } w=0.579n+2.57 \qquad (4.1)$$

where the unit of u and w is centimeter per second.

(2) Linearized output voltage from the hot film anemometer

The output voltage from Sensor 1 (Ch. 1) shows minima at wave crests and troughs while that from Sensor 2 (Ch. 2) shows maxima. In the same way, the output voltage from Sensor 2 shows

Table 4.1 Run designation

Series	Run	Probe position			Wave hight cm	Wave period s	Hot film calibration				Index Ref. (24)
		Hot film	propeller								
		z cm	z	Diretion			u_+	u_-	w_+	w_-	
I	H-1	−122	−122	Hori-zontal	110	2.50	2	1	5	5	
	H-2				38	2.50					
	H-3				83	2.07					8-C
	H-4				29	2.07					8-A
	H-5				41	1.47					9-C
	H-6				14	1.47					9-A
	H-7				61	4.65					6-A
	H-8				52	3.28					7-A
	H-9				105	3.28					7-C
	V-1	−122	−122	Ver-tical	110	2.50	4	3	6	6	
	V-2				38	2.50					
	V-3				83	2.07					8-C
	V-4				29	2.07					8-A
	V-5				41	1.47					9-C
	V-6				14	1.47					9-A
	V-7				61	4.65					6-A
	V-8				52	3.28					7-A
	V-9				105	3.28					7-C
II	H-1	−61	−61	Hori-zontal	110	2.50	8	7	9	9	
	H-2				38	2.50					
	H-3				83	2.07					8-C
	H-4				29	2.07					8-A
	H-5				41	1.47					9-C
	H-6				14	1.47					9-A
	H-7				61	4.65					6-A
	H-8				52	3.28					7-A
	H-9				105	3.28					7-C
	V-1	−61	−61	Ver-tical	110	2.50	8	7	10	10	
	V-2				38	2.50					
	V-3				83	2.07					8-C
	V-4				29	2.07					8-A
	V-5				41	1.47					9-C
	V-6				14	1.47					9-A
	V-7				61	4.65					6-A
	V-8				52	3.28					7-A
	V-9				405	3.28					7-C

Water depth h=335cm

Calibration curves (unit: u, w cm/s, E: volt)

1 : u=12.0E 2 : u=13.0E 3 : u=13.0E 4 : u=15.8E 5 : w=14.0E

6 : w=16.0E 7 : u=13.7E 8 : u=14.8E 9 : w=11.1E 10 : w=12.4E

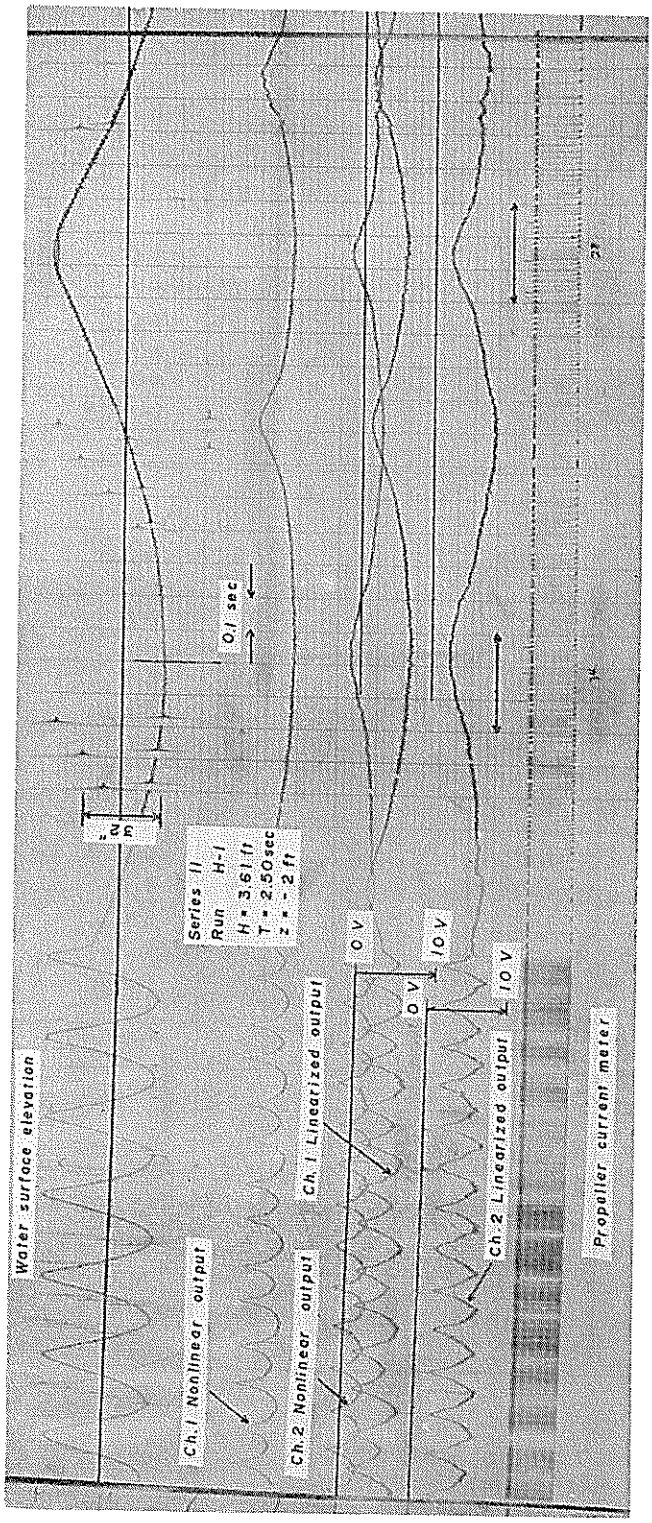

Photo 4.1 : Sample record

minima when the water surface crosses the still water level while that from Sensor 2 shows maxima there. Thus, the variations of the output voltage from Sensor 1 and Sensor 2 are respectively similar to that of the magnitude of the horizontal and the vertical velocity. However, it should be noted that the minimum output voltages are not zero, while wave theories predict that the minimum magnitude of each velocity component is zero. This should be caused by the effect of the tangential velocity component to the sensor axis.

It is said that the effective speed U_{eff} to cool a hot film sensor can be obtained from the relation[30]

$$U^2_{eff}=u_n^2+K^2u_t^2. \qquad (4.2)$$

where u_n is the normal velocity component to a sensor axis, u is the tangential velocity component and K is a value between 0.1 and 0.3 depending upon the magitude of the flow speed.

Hence, the output voltages in **Photo 4.1** result from contributions by both normal and tangential velocity comporents. These two contributions can be illustrated as shown in **Fig. 4.1.** It is seen that the contribuion of the tangential velocity is small or vanishes when the output voltage takes a maximum. The maximum velocities were reduced from the maximum output voltage using the corresponding calibration curves.

For the convenience of the expression, the

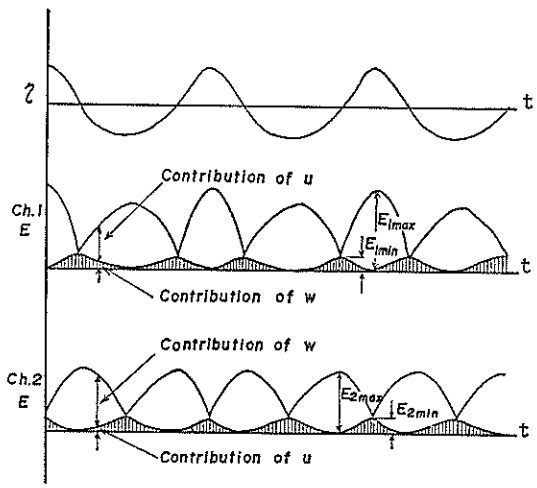

Fig. 4.1 : Illustration of linearized output voltage

following symbols are used to represent each maximum velocity.

u_+ : horizontal velocity beneath a wave crest

u_- : horizontal velocity beneath a wave trough

w_+ : vertical velocity when the water surface crosses the still water level upward

w_- : vertical velocity when the water surface crosses the still water level downward.

The hypothesis that the minimum output voltage was caused by the tangential velocity component was tested. The minimum voltage of each sensor was plotted as functions of the maximum tangential velocity (deduced from the maximum voltage from the other sensor) as shown in **Figs. 4.2** and **4.3**. It is seen that the minimum voltages $E_{1\min}$ and $E_{2\min}$ are linearly related to the magnitude of the maximum tangential velocities, w_+ and u_+. The relation are well expressed by the straight lines in these figures. The slope of these lines represent the directional coefficient $A(\theta)$ for $\theta=90°$ in **Eq.** (3.2). The ratio $A(90°)/A(0°)$ are consistent throughout the periodic wave tests (see **Table 4.2**).

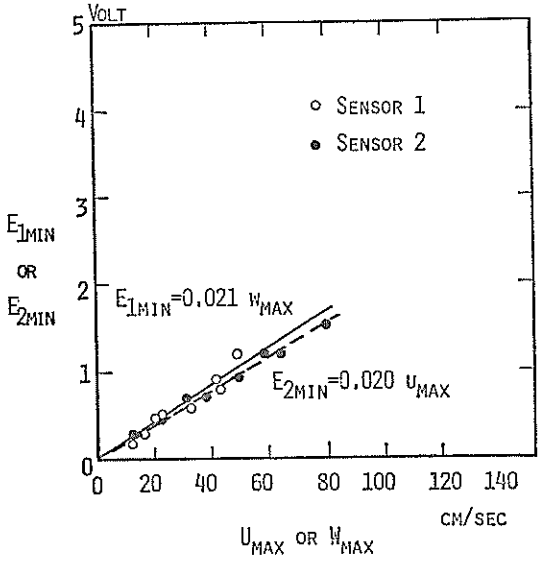

Fig. 4.2 : Hot film sensitivity to tangential velocity ($z=-122$cm).

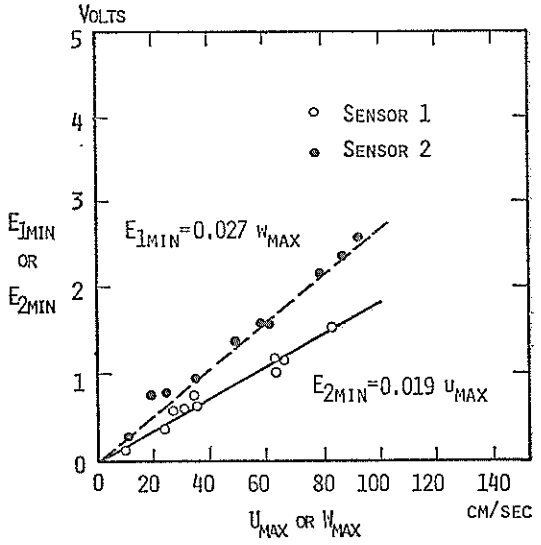

Fig. 4.3 : Hot film sensitivity to tangential velocity ($z=-61$cm).

Table 4.2 Directional coefficient A(θ)

Series	Sensor	$A(0°)$*	$A(90°)$**	$A(0°)/A(90°)$
I	Vertical sensor	2.07	0.57	0.27
	Horizontal sensor	2.76	0.82	0.30
II	Vertical sensor	2.35	0.64	0.27
	Horizontal sensor	2.18	0.60	0.28

* obtained from the calibration

** obtained from **Figs. 4.2** and **4.3**

As shown in **Table 4.1.** the water particle velocities were measured at the level of 0.61m and 1.22m below the still water level. In addition to these two levels, the velocities at the level of 0.30m below the still water level were measured with the hot film anemometer for some wave conditions. These additional tests were conducted with the interest in the hot film response when the probe was exposed to the air during the passage of the wave troughs.

Figure 4.4 shows a sample of these tests. The output voltage from both sensors suddenly become zero when the probe emerges out of water. They quickly recover as the probe submerges.

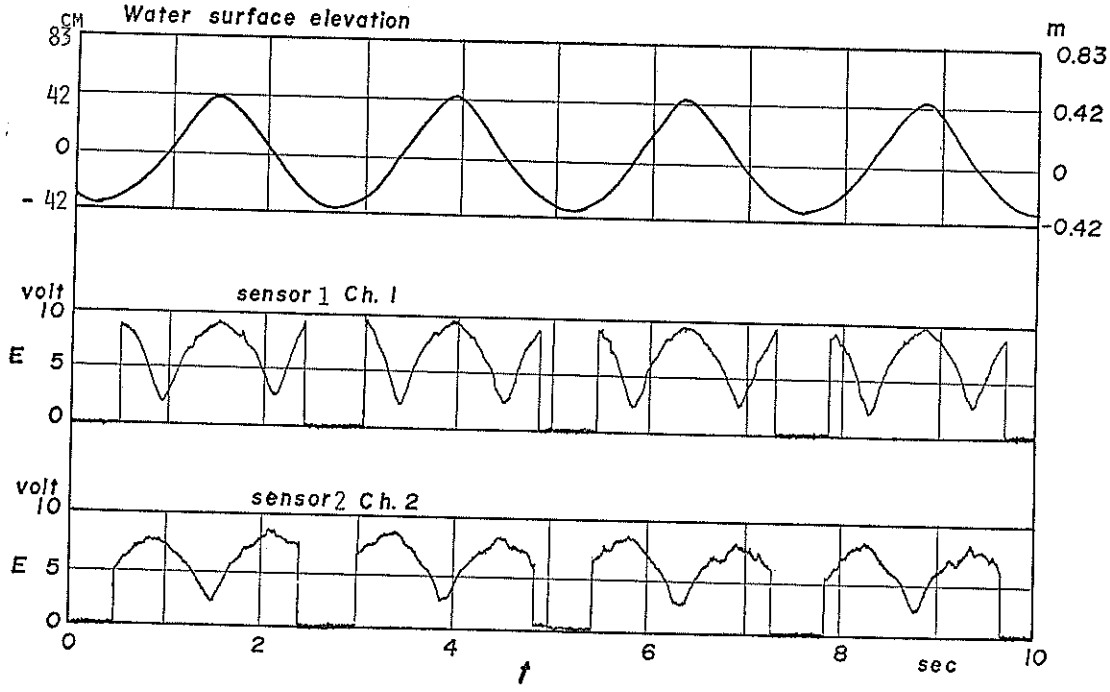

Fig. 4.4 : Sample recorp ($z=-30.5$cm, $H=83$cm, $T=2.5$s)

Table 4.3 Results of measurements and theretical prediction (unit:cm/s, $z=-122$cm)

Series	Run	Measurement								Theory								Airy**		Run
		Hot film				Propeller				Stokes 5th			Stream Function			Airy		See P. 26		
		u_+	u_-	w_+	w_-	u_+	u_-	w_+	w_-	u_+	u_-	w	u_+	u_-	w	u	w	u_+	u_-	
I	H-1	58.2	70.1	48.2	48.2	48.8	72.2			66.1	61.6	54.0				66.8	58.2	59.1	78.8	H-1
	H-2	25.3	28.7	16.2	20.7	25.9	23.8			23.2	22.9	19.8				23.2	20.4	22.1	24.4	H-2
	H-3	36.3	47.6	30.5	30.5	32.0	42.1			41.5	39.9	37.5	41.8	39.9	37.5	41.2	39.0	36.5	46.7	H-3
	H-4	14.3	17.4	14.3	14.3	16.5	14.9			14.0	14.0	13.1	14.0	14.0	13.1	14.0	13.4	13.7	14.9	H-4
	H-5	11.0	14.3	6.4	11.3	—	—			10.4	10.1	9.8	10.3	10.1	9.8	9.0	9.0	9.3	10.1	H-5
	H-6	3.1	2.7	2.4	2.4	—	—			3.1	3.1	3.1	3.1	3.1	3.1	3.1	3.1	3.0	3.1	H-6
	H-7	55.2	44.5	19.2	19.2	46.6	40.2			51.2	43.0	24.4	51.2	43.0	24.4	48.2	24.1	46.2	48.6	H-7
	H-8	44.2	40.2	24.1	24.1	36.0	35.0			38.1	36.0	25.6	39.0	36.0	25.6	37.2	26.2	35.5	38.6	H-8
	H-9	78.9	77.7	53.0	53.0	66.1	73.8			75.6	64.6	50.0	75.3	66.5	49.7	74.7	52.7	69.5	83.0	H-9
	V-1	58.2	63.7	50.3	55.8			50.6	46.0	66.1	61.6	54.0				66.8	58.2	59.1	78.8	V-1
	V-2	20.7	24.1	16.8	19.5			20.4	17.7	23.2	22.9	19.8				23.2	20.4	22.1	24.4	V-2
	V-3	31.1	45.7	35.1	35.1			20.1	33.2	41.5	39.9	37.5	41.8	39.9	37.5	41.2	39.0	36.5	46.7	V-3
	V-4	12.8	15.5	11.3	14.0			11.3	14.3	14.0	14.0	13.1	14.0	14.0	13.1	14.0	13.4	13.7	14.9	V-4
	V-5	5.2	11.9	7.0	9.8			—	—	10.4	10.1	9.8	10.3	10.1	9.8	9.0	9.0	9.3	10.1	V-5
	V-6	5.2	3.7	5.5	2.7			—	—	3.1	3.1	3.1	3.1	3.1	3.1	3.1	3.1	3.0	3.1	V-6
	V-7	50.6	42.1	22.3	18.3			24.4	24.7	51.2	43.0	24.4	51.2	43.0	24.4	48.2	24.1	46.2	48.6	V-7
	V-8	37.5	34.8	21.0	21.0			26.8	24.7	38.1	36.0	25.6	39.0	36.0	25.6	37.2	26.2	35.5	38.6	V-8
	V-9	64.6	63.7	39.0	43.3			46.9	48.8	75.6	64.6	50.5	75.3	66.5	49.7	74.7	52.7	69.5	83.0	V-9

Table 4.3 Result of measurements and theoretical prediction (unit:cm/s, $z=-61$cm) continued

Series	Run	Measurement								Theory								Airy**		Run
		Hot film				Propeller				Stokes 5th			Stream Function			Airy		See P. 26		
		u_+	u_-	w_+	w_-	u_+	u_-	w_+	w_-	u_+	u_-	w	u_+	u_-	w	u	w	u_+	u_-	
Ⅱ	H-1	79.8	87.5	78.6	78.6	63.0	66.1			93.0	81.4	81.1				96.0	89.9	79.8	132.8	H-1
	H-2	35.4	40.8	27.7	27.7	29.6	34.1			33.5	32.9	30.8				33.3	31.1	31.1	36.6	H-2
	H-3	61.9	75.0	66.5	66.5	56.4	64.0			68.6	64.6	63.7	68.6	64.3	63.7	71.4	69.8	59.9	95.5	H-3
	H-4	23.5	30.2	24.4	24.4	24.7	24.4			24.7	24.7	23.5	24.4	24.1	23.2	25.0	24.1	23.4	27.2	H-4
	H-5	25.0	31.4	27.7	22.3	20.7	25.9			28.7	27.7	27.4	29.9	28.7	28.4	28.7	28.4	25.1	31.6	H-5
	H-6	10.4	13.7	10.1	9.1	8.5	11.3			9.9	9.9	9.6	9.9	9.9	9.6	9.6	9.6	9.2	10.0	H-6
	H-7	59.1	60.1	33.2	24.4	48.8	54.6			57.0	46.0	32.6	57.0	46.0	32.6	52.7	32.0	50.0	54.3	H-7
	H-8	45.7	54.6	33.2	57.9	41.2	39.6			46.3	43.3	36.0	46.3	43.3	36.0	44.5	36.6	42.3	48.6	H-8
	H-9	84.1	94.2	67.4	67.4	77.4	79.6			92.7	77.4	69.8	92.4	78.0	69.5	90.0	73.5	81.3	108.7	H-9
	V-1	76.8	83.2	88.1	88.1			61.9	83.2	93.2	81.0	81.1				96.0	89.9	79.8	132.8	V-1
	V-2	35.4	40.8	38.4	33.5			31.4	30.5	33.5	32.9	30.8				33.3	31.4	31.1	36.6	V-2
	V-3	66.5	71.0	67.1	67.1			64.0	56.1	68.6	64.6	63.7	68.6	64.3	63.7	71.4	69.8	59.9	95.5	V-3
	V-4	29.6	30.2	27.4	22.3			26.5	22.0	24.7	24.7	23.5	24.4	24.1	23.2	25.0	24.1	23.4	27.2	V-4
	V-5	26.5	28.7	27.4	23.5			20.1	14.3	28.7	27.7	27.4	29.9	28.7	28.4	28.7	28.4	25.1	31.6	V-5
	V-6	10.4	12.2	13.7	11.3			9.8	11.0	9.9	9.9	9.6	9.9	9.9	9.6	9.6	9.6	9.2	10.0	V-6
	V-7	45.6	57.3	33.5	25.9			30.5	30.2	57.0	46.0	32.6	57.0	46.0	32.6	52.7	32.0	50.0	54.3	V-7
	V-8	45.7	53.3	37.2	37.2			34.4	36.9	46.3	43.3	36.0	46.3	43.3	36.0	44.5	36.6	42.3	48.6	V-8
	V-9	66.5	96.9	75.6	75.6			69.8	72.9	92.7	77.4	69.8	92.4	78.0	69.5	90.9	73.5	81.3	108.7	V-9

The output voltages show almost the same maximum values and profile for each individual wave. This shows that the effect of the probe exposure in the air to the sensor sensitivity, such as air bubbles adhering to the sensor surface, was small. Thus, the hot film probe can be operated near the still water level.

4.1.3 Measured velocities

The results of the periodic wave tests are summarized in **Table 4.3.** In this table, the velocities calculated from Stokes' fifth order theory[15], Dean's Stream Function theory[16] and Airy theory are listed.

The horizontal and vertical maximum velocities measured with the propeller current meter, $u_{\text{propeller}}$ and $w_{\text{propeller}}$, are compared with those measured with the hot film anemometer, $u_{\text{hot film}}$ and $w_{\text{hot film}}$, as shown in **Fig. 4.5** for each probe level, z. In the figure, the correlation coefficients,* of these measured velocities are shown. They are very lcose to 1.0 for all the cases. Hence, both the propeller and the hot film did function well. From the figure, it is seen that the velocities measured with the propeller current meter are smaller than those measured with the hot film anemometer.

The difference may be caused by the method of data processing. The frequency of the output pulses from the propeller current meter were averaged over from 0.2 to 0.3 seconds. Thus obtained maximum velocities may be smaller than the true maxium velocity, as more closely detected by the hot film anemometer.

4.1.4 Comparison with wave theories

As seen in **Table 4.3,** there are small differences among the theoritical values given by the wave theories. There is no practical difference between the velocities given by Stokes' fifth order theory

* The correlation coefficient of variables x and y is defined as

$$r_c=\frac{\sum\{(x-\bar{x})(y-\bar{y})\}}{\sqrt{\{\sum(x-\bar{x})^2\}\{\sum(y-\bar{y})^2\}}}$$

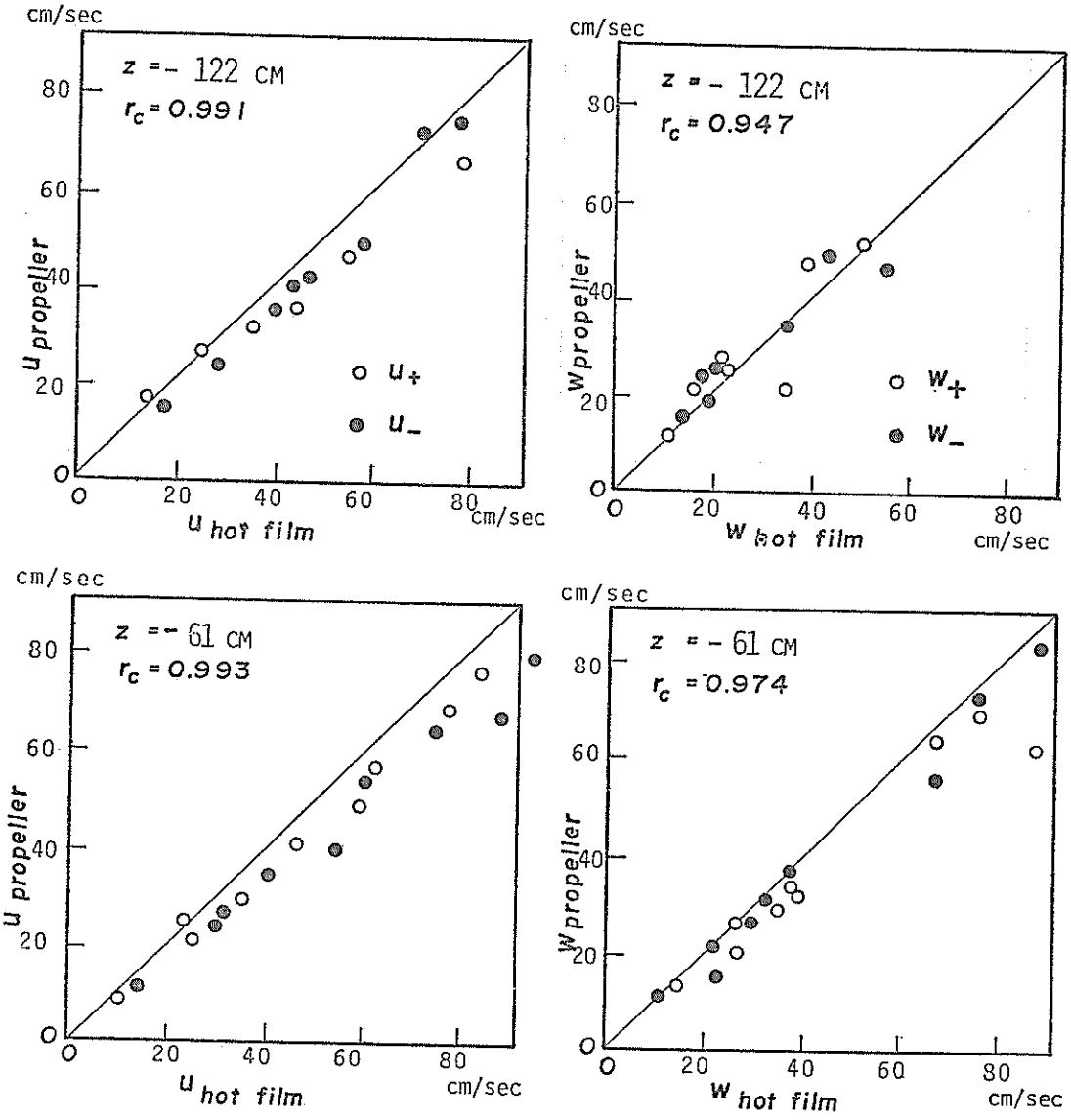

Fig. 4.5 : Correlation of the measured velocities and propeller and those measured with hot film

and those given by Dean's Stream Function Theory. Hence, the measured velocities are compared with the velocity distribution given by Stokes' fifth order theory and Airy theory for the cases that the latter theory gives notably different results from the former. The comparison are shown in **Figs. 4.6** through **4.14** for each wach wave condition. As a whole, the measured maximum velocities are very close to the theoretical velocity distributions.

The correlation coefficients of the measured velocity with the hot film anemometer and the theoretical velocities given by these two wave theories are also very close to 1.0 as shown in **Table 4.4**

The mean and the standard deviation of the relative error, r_p, defined by **Eq.** (4.3) are summarized in **Table 4.5.**

$$r_p = \frac{(u_+)_{\text{measured}} - (u_+)_{\text{theory}}}{(u_+)_{\text{theory}}}, \quad \text{etc.} \tag{4.3}$$

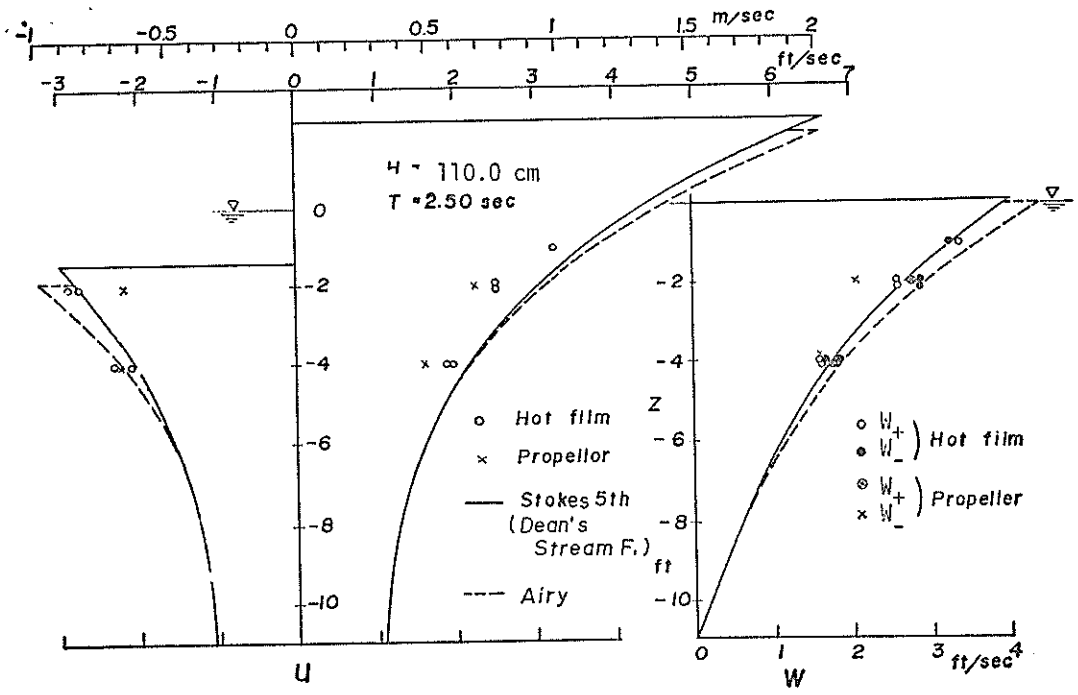

Fig. 4.6 : Comparison with theory (Run1)

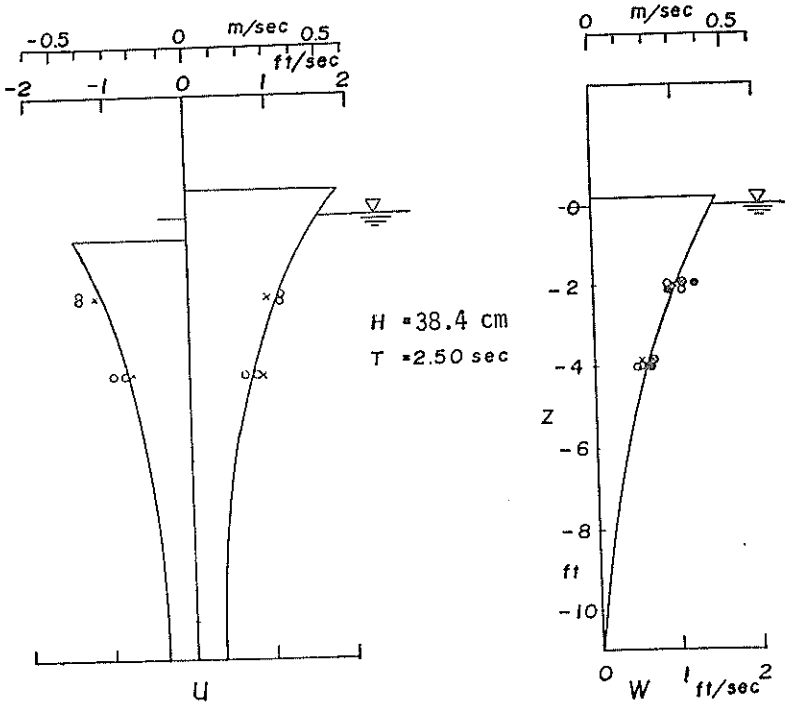

Fig. 4.7 : Comparison with theory (Run2)

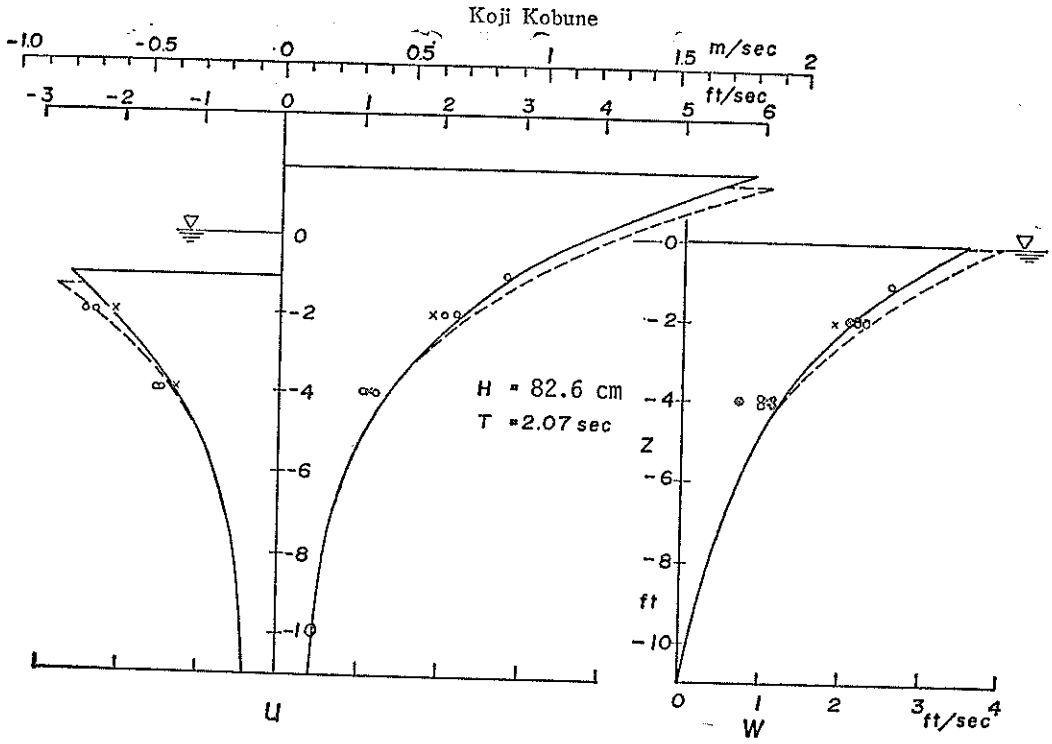

Fig. 4.8 : Comparison with theory (Run3)

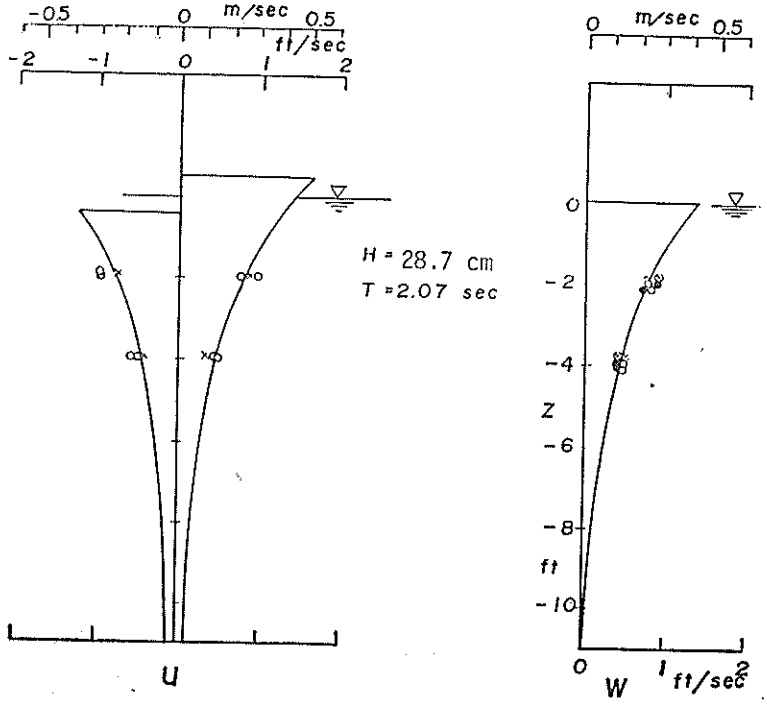

Fig. 4.9 : Comparison with theory (Run4)

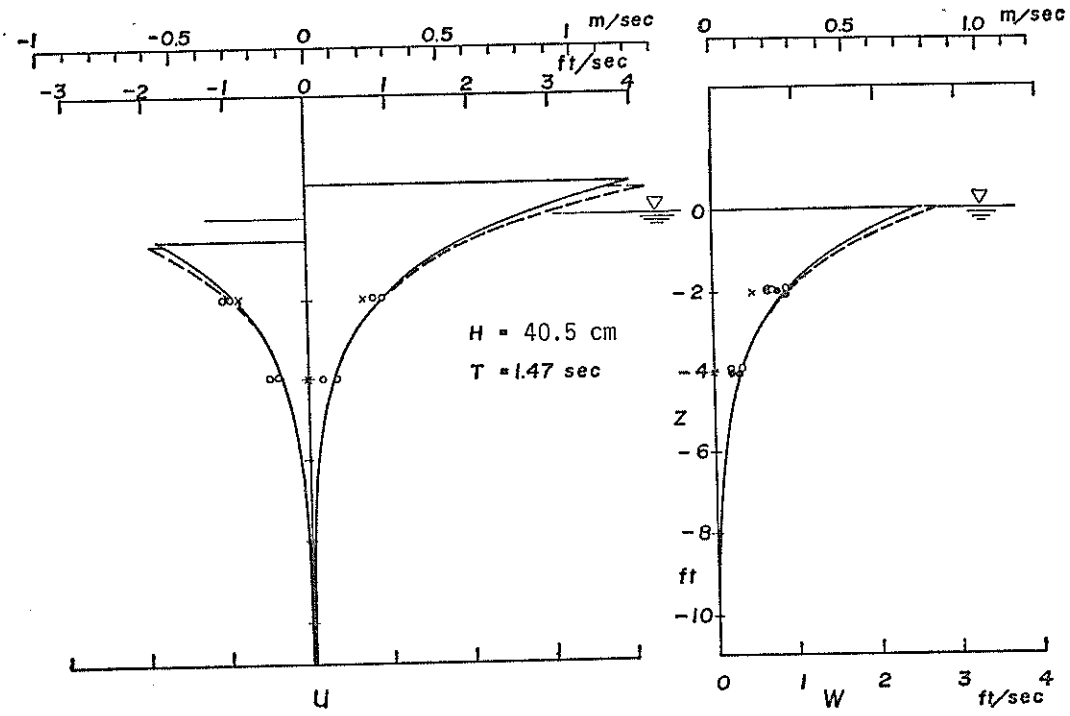

Fig. 4.10 : Comparison with theory (Run5)

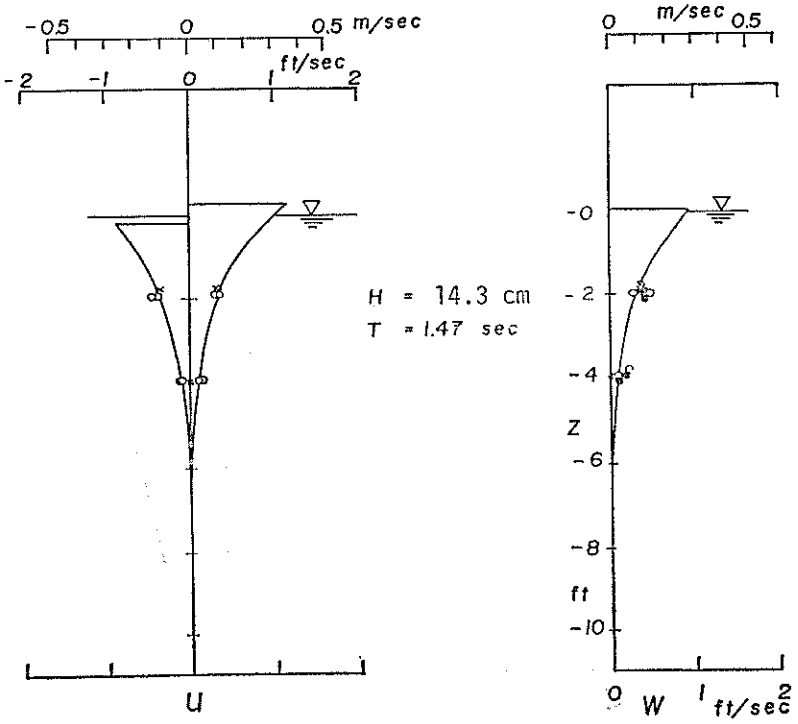

Fig. 4.11 : Comparison with theory (Run6)

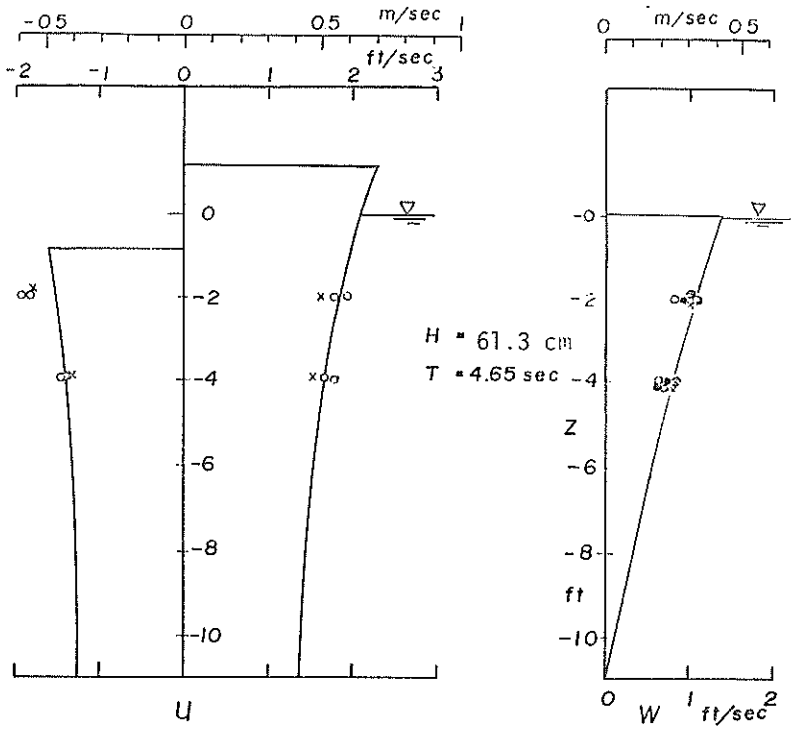

Fig. 4.12 : Comparison with theory (Run7)

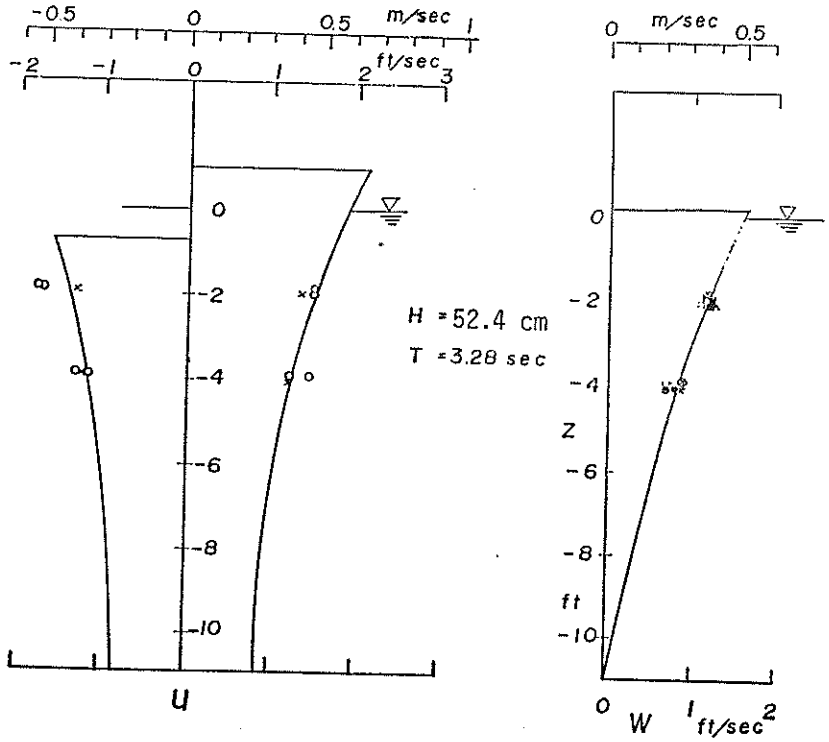

Fig. 4.13 : Comparison with theory (Run8)

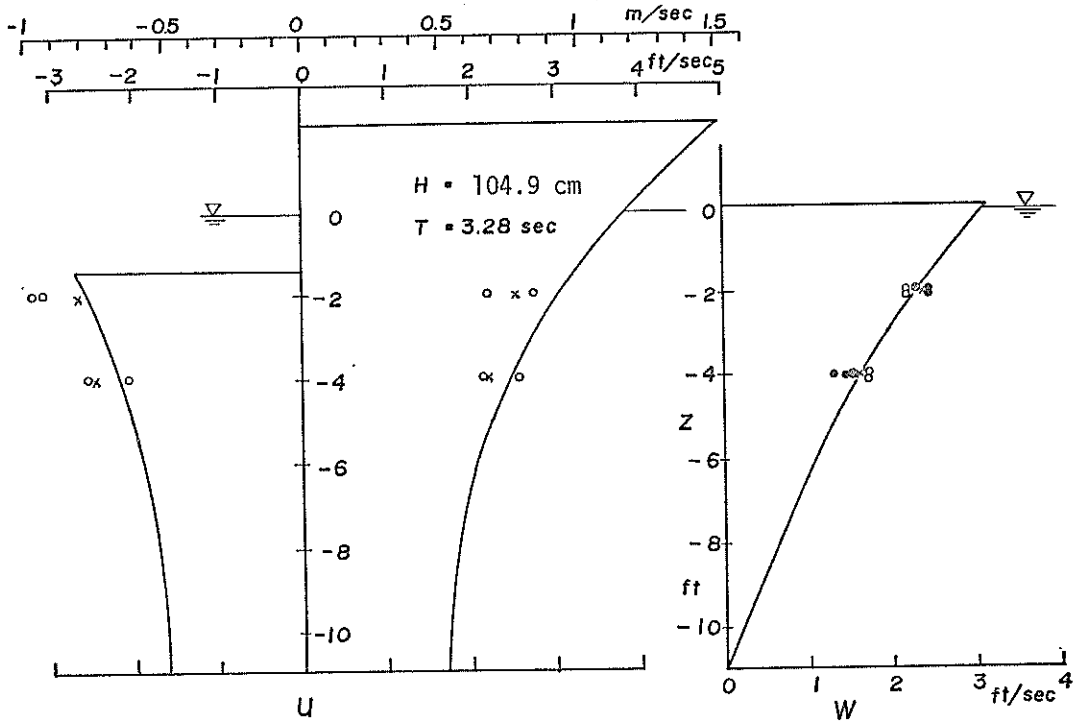

Fig. 4.14 : Comparison with theory (Run9)

Table 4.4 Correlation coefficient of the predicted and mfasured velocity (periodic wave)

Theory	Level z(cm)	r_C				Mean r_C
		u_+	u_-	w_+	w_-	
Stokes' 5th	−122	0.980	0.988	0.982	0.979	0.984
	−61	0.977	0.986	0.911	0.989	
Airy	−122	0.975	0.983	0.984	0.970	0.982
	−61	0.970	0.981	0.991	0.991	

Table 4.5 Relative error and standard deviation (periodic wave)

Theory	Level z(cm)	u_+	u_-	w_+	w_-
Stokes' 5th	−122	−0.032 (0.201)	0.110 (0.123)	−0.101 (0.211)	−0.071 (0.122)
	−61	−0.043 (0.106)	0.196 (0.089)	0.056 (0.115)	−0.031 (0.111)
Airy	−122	−0.025 (0.209)	0.059 (0.133)	−0.126 (0.213)	−0.098 (0.110)
	−61	−0.040 (0.116)	0.112 (0.120)	0.016 (0.117)	−0.070 (0.095)

Note : The numerals outside and inside the parenthesies represent the mean and standard deviation, respectively.

The prediction of the velocities with Stokes' fifth order theory yields almost the same means and standard deviations as the prediction with Airy theory. The means of the relative error show that the measured horizontal velocities beneath the wave crests are three to four percent smaller and those beneath the wave troughs are 10 to 20 percent larger than the theoretical predictions. On the other hand, the measured vertical velocities, in general, are smaller than the theoritical predictions for both w_+ and w_-. The standard deviations are varying from 0.1 to 0.2 at the level of -1.22m, and they are abou 0.1 at the level of -0.61m.

It is interesting that the measured horizontal velocity beneath the wave crests, u_+, are smaller, and those beneath the wave troughs, u_-, are larger than the predicted velocity from Airy theory. This shows that the magnitude of u_+ is smaller than u_-, since Airy theory gives equal magnitude for both u_+ and u_-, This is clearly seen in the measured velocity in **Table 4.3.** This tendency is a remarkable contrast with the theoritical results given by Stokes' fifth order theory and Dean's Stream Function Theory.

Many studies discuss the horizontal velocity beneath the wave crests of finite amplitude waves. However, there are few studies which show the velocities beneath the wave troughs. The experimental results reported by Goda[9] show that the horizontal velocities beneath the wave crests are smaller than those beneath the wave troughs for the most cases under intermediate water conditions (h/T^2 is larger than 25cm/s^2), while the opposite results are obtained for shallow water conditions (h/T^2 is less than 18cm/s^2). Iwagkai[13] showed the time variation of horizontal velocity was close to the higher order wave theory (Stokes' third order theory) rather than Airy theory, i.e. u_+ was larger than u_-. However, they measured only near bottom velocity and their test waves were relatively shallow water conditions (h/T^2 is less than 15 cm/s^2).

These variations of the velocity characteirstics may be caused according to the following reason. The water particle orbits are ellipses of which axes decrease according to the increase of the distance downward from the still water level. On the other hand, the wave theories approximate the velocity at the mean position of a water particle with the velocity on the orbit. A stationary probe does not trace the water particle. Beneath the wave crests, it measures the orbital velocity at the top of the orbit, the center of which is below the probe. On the other hand, beneath the wave troughs, it measures the orbital velocity at the bottom of the orbit, the center of which is above the probe. For given water depth and wave height, the axes of the elliptical water particle orbits are large as the distance away from the bottom increases. Therefore, the measured orbital velocity beneath the wave troughs may be larger than that beneath the wave crests.

The phenomenon stated above is illustrated in **Fig. 4.19.** Thus, the stationary probe at the level z may detect the larger orbtial velocity beneath wave crests and the smaller velocity beneath wave troughs.

Taking the water particle orbit into account, one can predict the orbital velocity beneath wave crest and trough at the level z. The maximum horizontal velocity at the level z is calculated from a wave theory as the velocity of the water particle of which mean position is z_c and which passes through the level z beneath the wave crest. In the same way. minimum horizontal velocity at the level z is calculated as the velocity of the water particle of which mean position is z_t and which passes through level z beneath the trough.

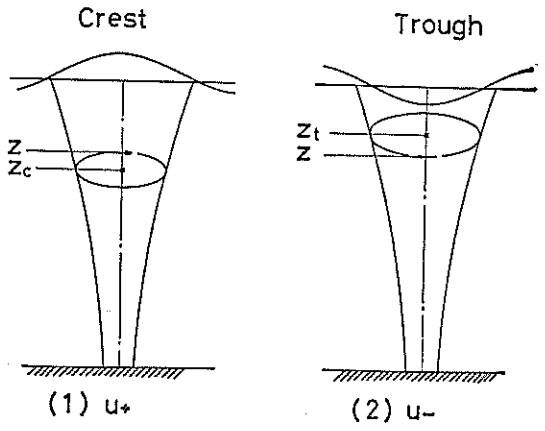

Fig. 4.19 : Sketch of a water particle orbit

Thus predicted maximum and mumimun horizontal velocities are shown in the columum Airy** in **Table 4.3.** These values have the same tendency as the measured horizontal velocities, and may

give an explanation of the phenomenon.

In addition, there should be non-linear effects due to a large wave motion. That is the orbital velocity of a water particle may be actually larger beneath the wave crest than that beneath the wave trough, even from Lagrangian stand point of view. Consequently, near breaking, the orbits are no longer closed ones. For detailed discussion, the water particle velocities should be measured at various levels over an entire cycle of the wave motion rather than the maximum velocities.

Though there are some difference between the measured and the predicted velocities as mentioned above, again, they are generelly less than 10 percent. The wave theory (either Stokes' fifth order theory, Dean's Stream Function Theory or Airy theory) provides good prediction of the velocities for the wave conditions in this study as seen in **Table. 4.5.**

4.2 Random wave

4.2.1 Wave conditions

Two kinds of wave spectra were employed in the random wave tests. The water particle velocities were measured mainly with the hot film anemometer at 61 cm and 122 cm below the still water level. The run designations are listed in **Table 4.6.** The random wave trains last about 160 seconds and they are composed of about 60 zero upcrossing waves. The zero upcrossing wave heights and periods were read with a scale from the record on oscillograph paper.

The relation between the heights and the periods of the zero upcrossing waves are plotted with dots in **Fig. 4.15** (spectrum I) and **Fig. 4.16** (spectrum II). As these figures show, Spectrum I is composed of steeper waves than Spectrum II and the range of the wave periods is about the same for both spectra. The wave conditions employed in the periodic wave tests are plotted with circles in **Fig. 4.15.** They cover most of the conditions associated with the discrete waves of the random waves.

The probability density and the cumulative probability of the wave heights are shown in **Fig. 4.17** and **Fig. 4.18.** respectively. They are fairly close to the Rayleigh distribution.

Table 4.6 Run designation (random wave)

Series	Run	Position of Hot film	Spectrum	Calibration curve			
				u_+	u_-	w_+	w_-
Ⅲ	1	−61cm	I	12	11	13	13
	2	−61	II				
	3	−122	I	15	14	16	16
	4	−122	II				

Water depth h=335cm

Calibration curve (Unit: u, w cm/s, E: volt)

11 u=8.56E　　12 u=9.17E

13 w=11.16E　　14 u=6.61E

15 u=8.47E　　16 w=10.00E

4.2.2 Wave spectrum

(1) Computation of the wave spectrum

Direct Fourier transformation of the time series $\eta(t)$ extending from t_1 to t_2 was computed to give the raw estimate of the power spectral density function at a frequency, f, as given by the following formula[27].

$$G_x(f)=\frac{2}{t_2-t_1}\left|X(f)\right|^2, \tag{4.4}$$

where $G_x(f)$ is the raw estimate of the power spectral density at the frequency f, and $X(f)$ is the Fourier transformation of the time series $\eta(t)$.

The Fourier transformation $X(f)$ is calculated from **Eq. (4.5).**

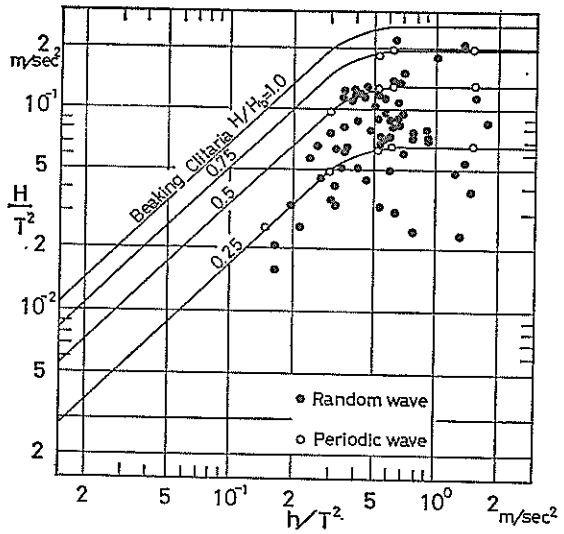

Fig. 4.15 : Discrete wave characteristics of random wave (Spectrum I)

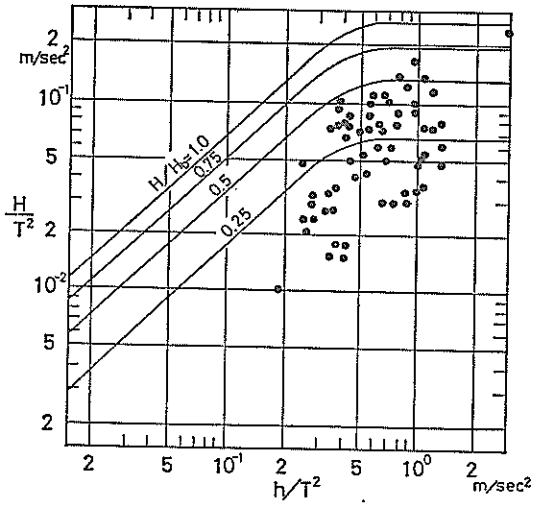

Fig. 4.16 : Discrete wave characteristics of random wave (Spectrum II)

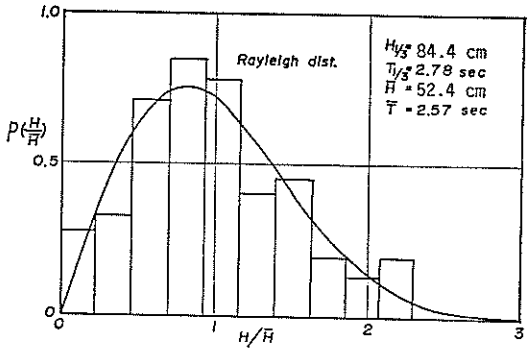

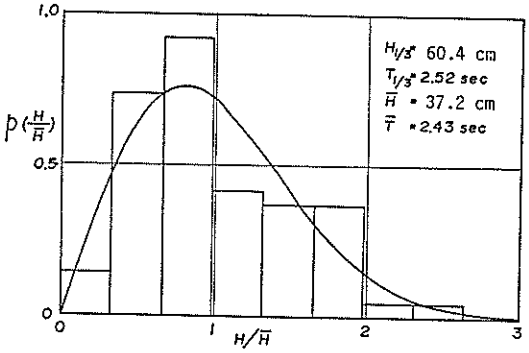

Fig. 4.17 : Probability density of wave height

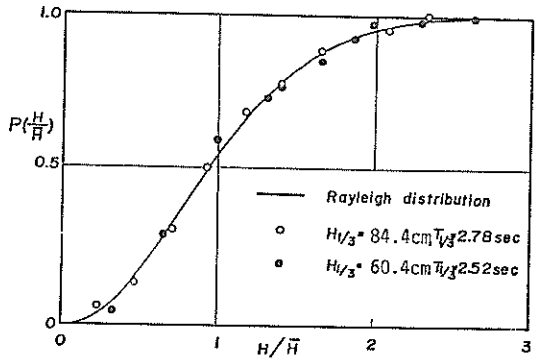

Fig. 4.18 : Wave height distribution

$$X(f)=\int_{-\infty}^{\infty}\eta(t)\ e^{-j2\pi ft}dt \tag{4.5}$$

For the practical calculation for a discrete record $\eta(t_m)$, $m=1, 2, 3, \cdots, N$, at a time interval τ, **Eq.** (4.5) is rewritten into

$$X(f)=\tau\sum_{m=1}^{N}[\eta(t_m)\cos(2\pi fm\tau)-j\ \sin(2\pi fm\tau)]=A(f)-jB(f) \tag{4.6}$$

where $t_2-t_1=N\tau$ (4.7)

$$A(f)=\tau\sum_{m=1}^{N}\eta(t_m)\cos(2\pi fm\tau) \tag{4.8}$$

$$B(f)=\tau\sum_{m=1}^{N}\eta(t_m)\ \sin(2\pi f m\tau). \tag{4.9}$$

Hence, the raw estimate of the spectral density, $G_x(f)$ is calculated by

$$G_x(f)=\frac{2}{t_2-t_1}[A(f)^2+B(f)^2]. \tag{4.10}$$

The parameters employed in the practical computations are as follows.
$N=1546$, $\tau=0.1$ sec and $f=0.2$ through 1.4 sec^{-2} (at an interval 0.01 sec^{-1})
The raw estimates $G_x(f)$ are smoothed with the use of a boxcar function, Eq. (4.11).

$$\tilde{G}_x(f_m)=\frac{1}{10}[G_x(f_{m-5})+G_x(f_{m-4})+\cdots\cdots+G_x(f_{m+4})] \tag{4.11}$$

(2) Comparison with the Bretschneider spectrum
The Bretschneider spectrum is given by the fnllowing formula for a fully developed sea[33].

$$S_H{}^2(\omega)=3.437\frac{\bar{H}^2}{\bar{\omega}}\left(\frac{\bar{\omega}}{\omega}\right)^5 e^{-0.675\left(\frac{\bar{\omega}}{\omega}\right)^4} \tag{4.12}$$

where $\bar{\omega}=2\pi/\bar{T}$
The Bretschneider spectrum implies the following relationship.

$$\bar{H}^2=8\overline{\eta^2(t)}=\int_0^\infty S_{H2}(\omega)\ d\omega \tag{4.13}$$

This should be carefully distiguished from

$$\eta^2(t)=m_0=\int_0^\infty S_{\eta\eta}(f)\ df \tag{4.14}$$

where m_0 is the zeroth moment of $S_{\eta\eta}(f)$ about the origin.
From these two equations, the Bretschneider spectrum, $S_{H2}(\omega)$ is transformed into the common expression of wave spectrum as follows.

$$[S_{\eta\eta}(f)]_{\text{Bretschneider}}=\frac{2[S_H{}^2(\omega)_{\text{Bretschneider}}]}{8} \tag{4.15}$$

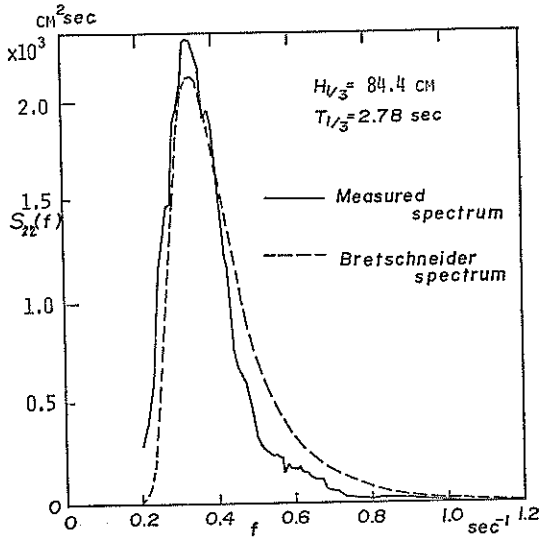

Fig. 4.20 : Wave spectrum (Spectrum I)

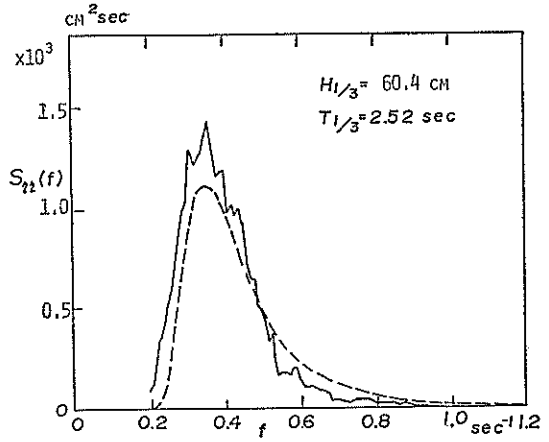

Fig. 4.21 : Wave spectrum (Spectrum II)

Figures 4.19 and **4.20** show the comparison of the measured spectrum with Bretschneider spectrum. In the computation of Bretschneider spectrum, the parameter $\eta^2(t)$ and $\bar{T}$ obtained from the time series $\eta(t)$ are used to give the values, $\bar{H}$ and ω, in **Eq.** (4.12). For both cases, the spectrum of the test random waves show a close similarity to the Bretschneider spectrum, though the measured spectrum has some what larger density in the lower frequency range, and smaller density in the higher frequency range.

The parameters associated with the measured spectra are summarized in **Table 4.7**. The significant wave heights, $H_{1/3}$, the mean wave heights, $\bar{H}$, and the mean wave periods, $\bar{T}$, which were computed from the moments of the measured spectra[28], are close to those calculated from zero upcrossing wave readings.

Table 4.7 Parameters of test random waves

Parameter	Spectrum I	Spectrum II
m_0	0.4898	0.3517
m_2	0.07619	0.06179
m_4	0.02078	0.01860
ε^2	0.4300	0.4164
ε	0.656	0.645
$H_{1/3}$ (cm)	85.3 (84.4)	72.2 (60.5)
$\bar{H}$ (cm)	53.3 (52.4)	45.1 (37.2)
$T_{1/3}$ (s)	(2.78)	(25.2)
$\bar{T}$ (s)	2.54 (2.57)	2.39 (2.43)

Note : The numerals outside and inside the parentheses represent the value obtained from the measured spectrum and the value obtained from the direct reduction of zero upcrossing wave height and period, respectively.

4.2.3 Sample data of velocity measurement

Figure 4.22 shows a sample record. Generally, the maxima of the output voltage from Sensor 1 (Ch. 1) appear beneath the wave crests and the troughs while the output voltage from Sensor 2

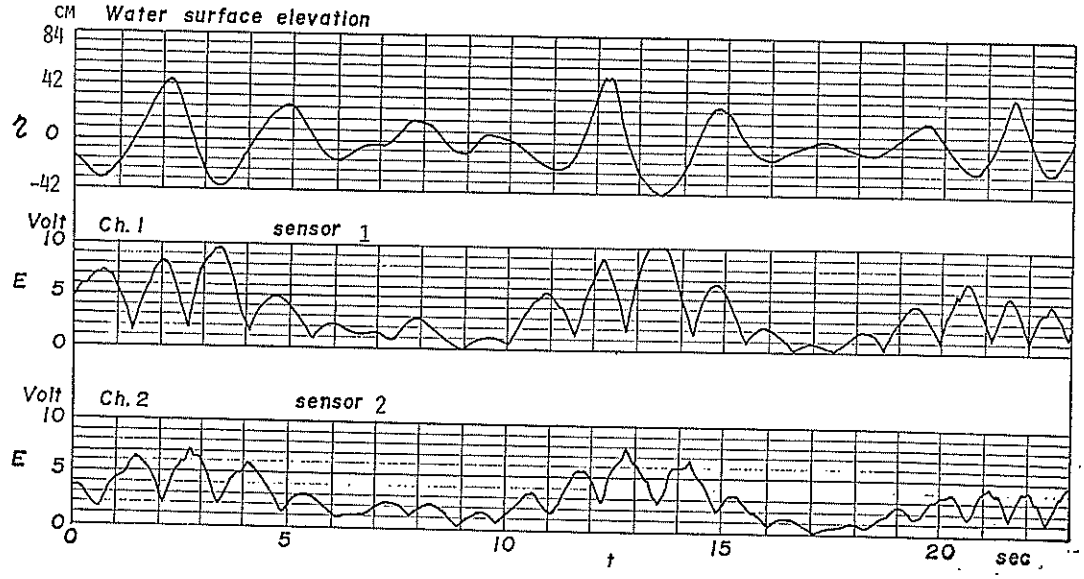

Fig. 4.22 : Sample record of random wave test (Spectrum II)

(Ch. 2) shows its minima there. The maxima of Ch. 2 apper when the water surface crosses the still water level while the output of Ch. 1 shows the minima there. These aspects are clearly seen for large waves, and have the same general characteristics as observed in the periodic wave tests. Thus, the maximum values of the horizontal and vertical velocity components can be measured in the same way as in the periodic wave tests.

Figures 4.23. and **4.24** show the correlation of the horizontal and vertical velocities in random wave measured with the propeller current meter and those measured with the hot film anemometer. The correlation of these two measured velocities with different apparatuses is fairly good for both horizontal and vertical velocities.

As discussed in **Appedix A,** the propeller current meter is sensitive only to the velocity component of which direction is parallel to the propeller spindle. Thus, the velocity detected by the propeller is not affected by the transverse velocity component. On the other hand, the velocity detected by the hot film sensors may be contaminated by the transverse velocity component, if any. However, the correlation coefficients are very close to 1.0 and the relation between two measured velocities can be aperoximated by

$$u = u_{\text{hot film}} \tag{4.16}$$

on the average. This confirms the effect of the transverse velocity component on the normal velocity component is very small even in random wave, when the output voltage from either Sensor 1 or Sensor 2 shows its maxima.

Hence, for the convenience of the data processing, the velocity measured with the hot film anemometer is analyzed in the following chapter.

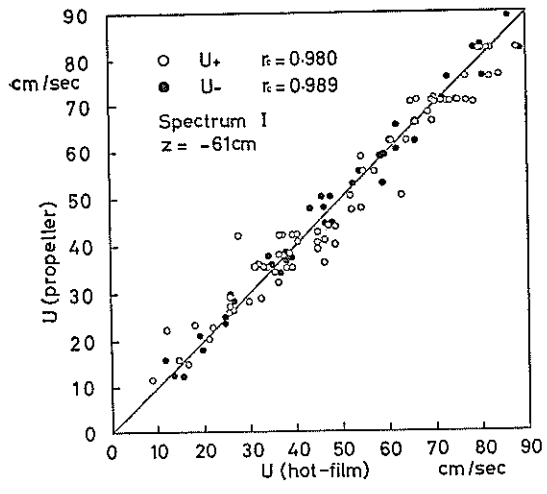

Fig. 4.23 : Correlation of velocities measured with propeller and hot film (horizontal velocity)

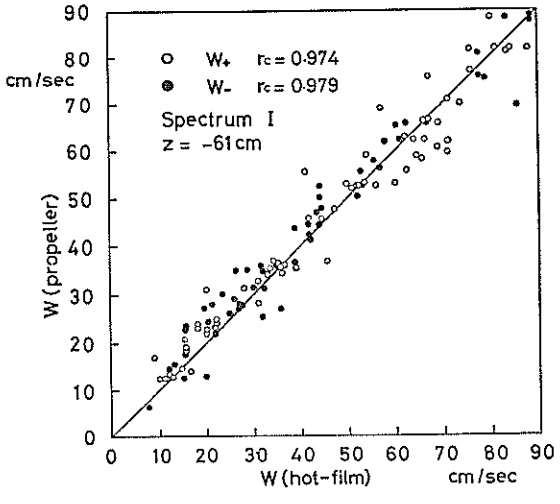

Fig. 4.24 : Correlation of velocities measured with propeller and hot film (vertical velocity)

5 Estimation of velocities in random waves

5.1 Statistical estimation through spectrum analysis

On the basis of Airy theory (linear wave theroy), the horizontal velocity and the verical velocity at a location are given by the following complex functions,

$$u(t) = a\omega \frac{\cosh k(z+h)}{\sinh kh} e^{j(kx-\omega t)} \tag{5.1}$$

$$w(t)=-ja\omega\frac{\sinh\ k(z+h)}{\sinh\ kh}e^{j(kx-\omega t)} \tag{5.2}$$

while the water surface elevation is given by

$$\eta(t)=ae^{j(kx-\omega t)}, \tag{5.3}$$

where a is the amplitude of the surface elevation ($a=H/2$) and $\omega=2\pi f=2\pi/T$, with T the wave period. Hence, the relation of the horizonal and vertical velocity to the water surface elevation are written as

$$u(t)=R'_u\ (f)\ \eta(t) \tag{5.4}$$

$$w(t)=R'_w(f)\ \eta(t), \tag{5.5}$$

where

$$R'_u(f)=2\pi f\frac{\cosh\ k(z+h)}{\sinh\ kh} \tag{5.6}$$

$$R'_w(f)=-2\pi jf\frac{\sinh\ k(z+h)}{\sinh\ kh}. \tag{5.7}$$

The functions $R'_u(f)$ and $R'_w(f)$ are called the frequency response functions. For the given location, they are functions of only frequency, not functions of time.

The velocities $u(t)$ and $w(t)$ are thus linearly related to the water surface elevation. There are the following interrelationships between the spectral density of the horizontal velocity, $u(t)$, or the vertical velocity, $w(t)$, and that of the surface elevation[31].

$$S_{uu}(f)=|R'_u(f)|^2S_{\eta\eta}(f) \tag{5.8}$$

$$S_{ww}(f)=|R'_w(f)|^2S_{\eta\eta}(f) \tag{5.9}$$

where $S_{uu}(f)$ is the spectral density of the horizontal velocity fluctuation and $S_{ww}(f)$ is the spectral density of the vertical velocity fluctuation. Utilizing the above two equations, the velocity spectra are estimated from a given wave spectrum.

Once the velocity spectra $S_{uu}(f)$ and $S_{ww}(f)$ are obtained, the probability density of maximum velocities and the mean interval of zero upcrossings associated with the random variation of the velocities, with the use of the following equation presented by Cartwright and Longuet-Higgins[28].

i) Probability density of maxima

$$p(x_m)=\frac{1}{\sqrt{2\pi m_0}}\left[\varepsilon\ \exp\left(-\frac{x_m^2}{2\varepsilon m_0}\right)\right.$$
$$\left.+(1-\varepsilon)^{1/2}\frac{x_m}{\sqrt{m_0}}\exp\left(-\frac{x^2_m}{2}\right)\int_{-\infty}^{\frac{x_m}{\sqrt{m_0}}\frac{(1-\varepsilon^2)^{1/2}}{\varepsilon}}\exp\left(-\frac{x^2}{2}\right)dx\right] \tag{5.10}$$

where $p(x_m)$ is the probability density of x_m, x_m is the maximum values of random function $x(t)$, ε is the spectral width defined as

$$\varepsilon^2=\frac{m_0m_4-m_2^2}{m_0m_4} \tag{5.11}$$

and m_ν is the νth moment of the spectrum about the origin, i.e.

$$m_\nu=(2\pi)^\nu\int_0^\infty f^\nu S_{xx}(f)\ df, \tag{5.12}$$

where $S_{xx}(f)$ is the spectral density funsion of $x(t)$.

ii) Mean interval of zero upcrossing

$$\bar{T}=2\pi(m_0/m_2)^{\frac{1}{2}} \tag{5.13}$$

Figures 5.1 and **5.2** show velocity spectra from the operation of **Eqs.** (5.8) and (5.9') for the horizontal and vertical velocity, respectively. The response functions $R'_u(f)$ and $R'_w(f)$ are also plotted on these figures. The frequency response functions $R'_u(f)$ and $R'_w(f)$ behave as filters which

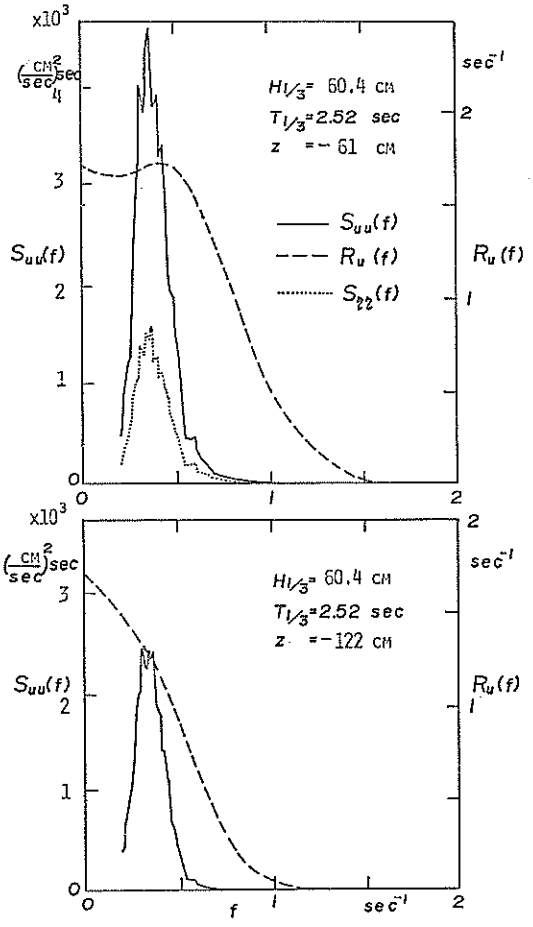

Fig. 5.1 : Velocity spectrum (horizontal velocity)

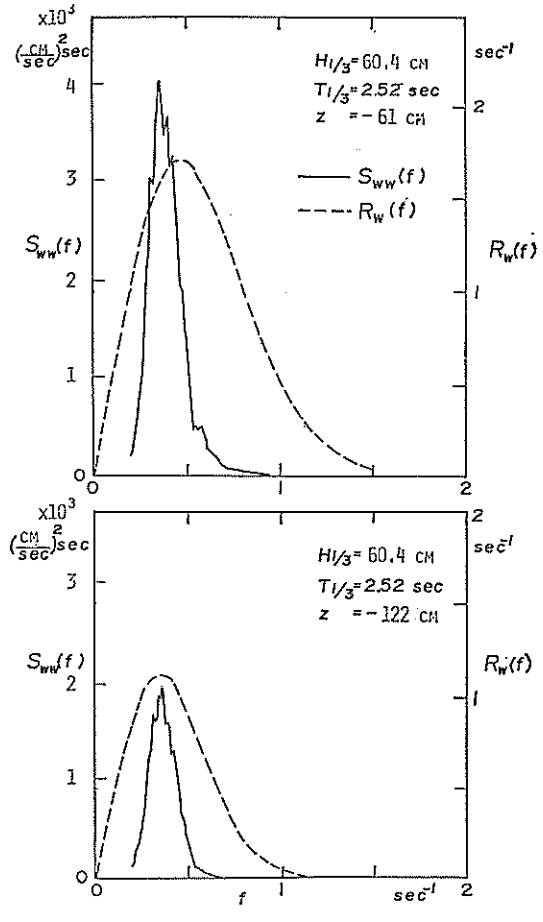

Fig. 5.2 : Velocity spectrum (vertical velocity)

attenuate the contribution of wave spectrum $S_{\eta\eta}(f)$ to the velocity spectra $S_{uu}(f)$ and $S_{ww}(f)$ for the higher frequency range, and which amplify it for the frequency range about the peak of $S_{\eta\eta}(f)$. The resultant velocity spectra thus become narrower banded spectra than the wave spectra.

The band width of a spectrum is characterized by a parameter, ε, which is calculated from **Eq.** (5.11). The parameter ε of the the computed velocity spectra and zeroth, second and fourth moments of it are listed in **Table 5.1** for Spectrum I and in **Table 5.2** for Spectrum II. These tables show

Table 5.1 Characteristic values of velocity spectrum
(Spectrum I, $H_{1/3}$=84.4cm, $T_{1/3}$=2.78 s)

	u		w		η
	z=−61cm	z=−122cm	z=−61cm	z=−122cm	
m_0	1.3904	0.7287	1.1369	0.5322	0.4898
m_2	0.1969	0.08729	0.1734	0.01959	0.07619
m_4	0.03750	0.01276	0.0350	0.01095	0.02078
ε	0.507	0.495	0.495	0.411	0.656

Table 5.2 Characteristic values of velocity spectrum (Spectrum Ⅱ, $H_{1/3}$=60.4cm, $T_{1/3}$=2.52s)

	u		w		η
	z=−61cm	z=−122cm	z=−61cm	z=−122cm	
m_0	0.9957	0.4872	0.8478	0.3740	0.3517
m_2	0.1572	0.06464	0.1426	0.05378	0.06179
m_4	0.03256	0.01040	0.03091	0.009213	0.01860
ε	0.388	0.419	0.474	0.401	0.645

that the spectral widths of velocity spectra fall within the range from 0.4 to 0.5 while the spectral width of the wave spectrum is about 0.65 for both spectra. The former is obviously smaller than the latter.

For a value of ε smaller 0.5, the probability density, **Eq.** (5.10), is very close to the Rayleigh distribution, which corresponds to the case ε=0. As a matter of fact, the probability distribution of the measured maxima of the horizontal velocity shows good agreement with the Rayleigh distribution as shown in **Fig. 5.3.**

Thus the probability distribtion of the maximum velocity can be approximated by the Rayleigh distribution:

$$p(u_{\max})=\frac{u_{\max}}{m_0}\exp(-u_{\max}^2/2m_0). \quad (5.14)$$

This distribution yields the following relations among charactic values of $u_{\max}$[29].

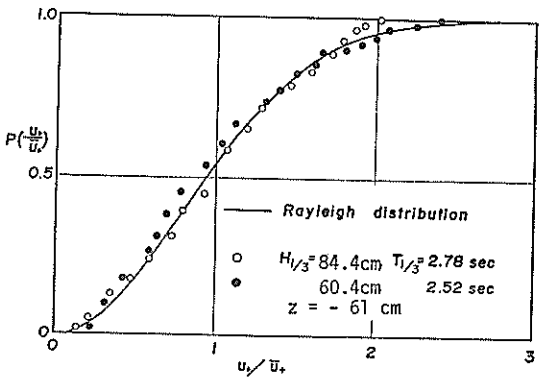

Fig. 5.3 : Probability distribution of the velocity beneath wave crests

$$\begin{aligned} u_{1/10}/\sqrt{m_0}&=2.55\\ u_{1/3}/\sqrt{m_0}&=2.0\\ \bar{u}/\sqrt{m_0}&=1.25 \end{aligned} \quad (5.15)$$

where $m_0=\overline{u^2(t)}$.

These theoretical results are summarized together with the experimental results as listed in **Table 5.3.**

Consider the relative error of the statistical velocity estimates by the following definition:

$$r_s=\frac{(u_{1/l})_{\text{measured}}-(u_{1/l})_{\text{predicted}}}{(u_{1/l})_{\text{predicted}}} \quad (5.15)$$

where $u_{1/l}$ is the mean of one-lth largest maximum velocities. The relative errors calculated from the values in **Table 5.3** are plotted on **Fig. 5.4** for each run. The range of the relative error is from −0.2 to 0.2.

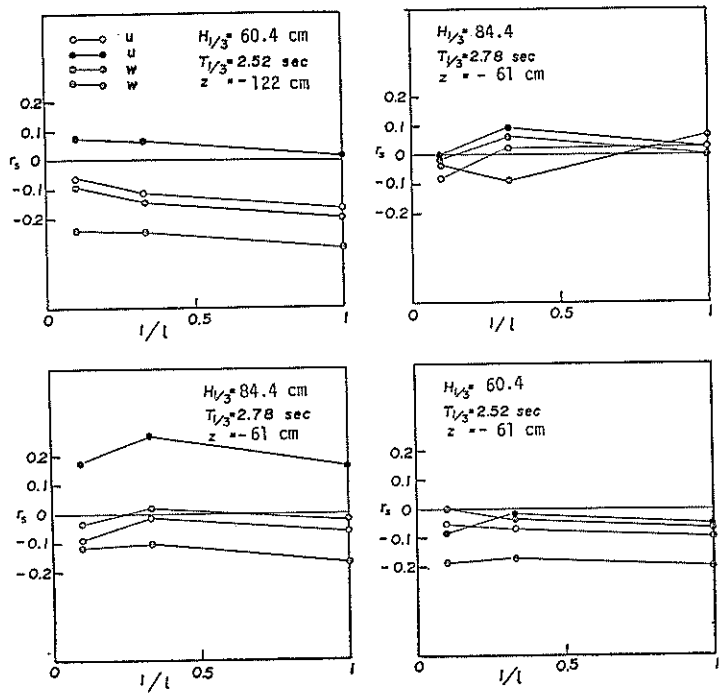

Fig. 5.4 : Relative error of statistical estimation

Tabl 5.3 Statistical estimation of velocity

Spectrum	$H_{1/3}$ (cm)	$T_{1/3}$ (s)	z (cm)	velocity	Experiment			Theory		
					$u_{1/10}$	$u_{1/3}$	$\bar{u}$	$u_{1/10}$	$u_{1/3}$	$\bar{u}$
I	84.4	2.78	−61	u_+	84.1	73.8	46.0	91.7	71.9	44.8
				u_-	92.4	78.0	46.0	〃	〃	〃
				w_+	68.9	71.0	43.0	82.9	64.9	40.5
				w_-	84.4	68.6	40.2	〃	〃	〃
			−122	u_+	60.4	51.5	30.5	66.5	52.1	32.6
				u_-	78.3	65.8	37.8	〃	〃	〃
				w_+	71.6	45.1	27.1	56.7	44.5	27.7
				w_-	50.0	39.9	22.9	〃	〃	〃
II	60.4	2.54	−61	u_+	72.9	56.7	34.4	77.4	61.0	38.1
				u_-	71.2	59.7	36.0	〃	〃	〃
				w_+	71.6	54.6	32.6	71.6	56.1	35.1
				w_-	57.9	46.3	28.0	〃	〃	〃
			−122	u_+	50.6	37.5	22.0	54.3	42.7	26.5
				u_-	58.5	45.4	26.2	〃	〃	〃
				w_+	43.3	31.7	18.6	47.6	37.2	23.2
				w_-	36.0	20.0	16.2	〃	〃	〃

(Unit:cm/s)

5.2 Estimation by simple application of periodic wave theory

In this section, the relation of discrete waves in random wave to a theoretical wave model is examined from the view point of the maximum water particle velocities.

5.2.1 Theoretical wave model

As discussed in **Chapter 4.2** and compared in **Table 4.3**, for the level −0.6 and −1.22m and the test wave conditions, the maximum velocities predicted from Airy theory are very close to those predicted from the higher order wave theories: Stokes' fifth order theory and Dean's Stream Function theory*. In addition, as compared in **Table 4.5**, there is no practical difference in the means and the standard deviation of the relative error, r_r, whichever theory is used to predict the maximum velocities.

Thus, Airy theory gives a good approximation to the higher order theories. Hence, for the convenience of the computation, Airy theory is used to predict velocities of each discrete waves in a random wave train.

5.2.2 Prediction of velocity

From each zero upcrossing wave hight and period, the maximum velocties at the level z are calculated as follows with the aid of Airy theory.

$$(u_{\text{predicted}})_i = |R'_u{}^1(f_i)|H_i/2$$
$$(w_{\text{predicted}})_i = |R'_w{}^1(f_i)|H_i/2 \qquad (5.16)$$

where $f_i=1/T_i$ are zero upcrossing wave height and period of ith wave.

The correlation of thus predicted velocities and the observed velocities of the discete waves are shown in **Figs. 5.5** and **5.6** for the case of Spectrum I at the level $z=-1.22$m. **Figure 5.5** shows the correlation of the horizontal velocities, and **Fig. 5.6** shows the correlation of the vertical velocities. As seen in these figures, the relations between the observed and the predicted velocities

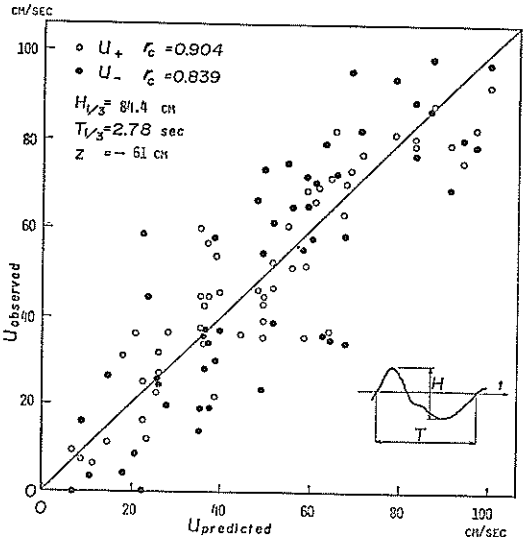

Fig. 5.5 : Comparison between predicted and observed velocity (horizontal velocity)

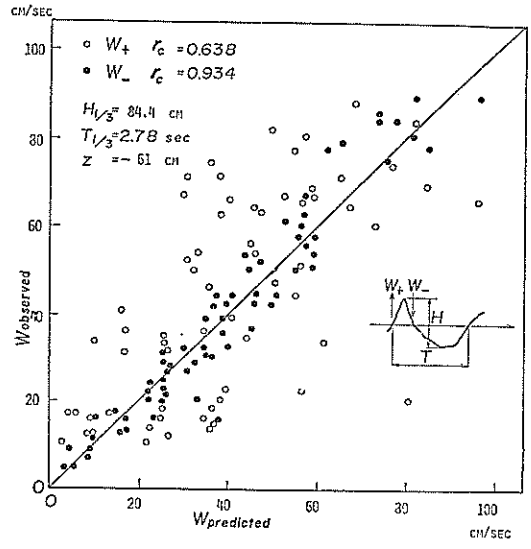

Fig. 5.6 : Comparison between predicted and observed velocity (vertical velocity)

* This does not imply that the velocities predicted by Airy theory are close to those predicted by the higher order theories over an entire cycle of the wave motion. Above discussion holds only for the maximum velocities.

of the discrete waves widely scatter. Among the four maximum velocities, u_+, u_-, w_+, w_-, the extent of the scattering is relatively small for w_-.

The large scattering is probably from the asymmetric water surface profile about the still water level. One asymmetry is the nonlinear wave profile which is charaterized by a steep crest and a flat trough. Another is caused by the irregularity of the water surface fluctuation, i.e., the fact that large crests are not always followed by large troughs and small crests are not always followed by small troughs.

As examined in the previous chapter, the effect due to the non-linear profile is supposed to be small. Hence, the difference between the observed and predicted velocities is mainly caused by the asymmetry of the wave profile due to the irregular water surface motion.

The extents of the scattering are quantitatively expressed by correlation coefficients. The correlation coefficients for all the runs are summarized as shown in **Table 5.4**, together with the coefficients, a and b, of the linear regression equation (5.17) computed by least-squares method.

$$(u_+)_{\text{observed}} = a(u_+)_{\text{predicted}} + b, \quad etc. \tag{5.17}$$

Table 5.4 Correlation coefficients and linear regression line (random wave)

Level z(cm)	Velocity	Spectrum I			Spectrum II		
		r_c	a	b	r_c	a	b
−122	u_+	0.803	0.756	0.165	0.873	0.879	0.069
	u_-	0.760	0.939	0.216	0.820	0.980	0.127
	w_+	0.633	0.657	0.309	0.763	0.842	0.066
	w_-	0.956	0.925	0.047	0.889	0.869	−0.009
−61	u_+	0.904	1.003	0.010	0.904	1.039	0.048
	u_-	0.839	1.017	0.054	0.740	1.067	0.019
	w_+	0.638	0.985	0.051	0.606	0.982	0.110
	w_-	0.934	1.005	0.010	0.931	0.922	0.007

From **Table 5.4**, the correlation coefficients u_+ and u_- are almost equvalent and they are ranging from 0.8 to 0.9. The correlation coefficients of w_+ and w_- show a contrast. That is, the coefficients of w_+ are about 0.6 for most cases while those of w_- about 0.9.

Such a difference results from the definition of the wave height and period which are used to predit the vertical velocities. The maximum velocity w_- is observed within a zero upcrossing wave. On the other hand, w_+ is observed inbetween two adjacent zero upcrossing waves. Therefore, the zero upcrossing wave heights and periods (crest to trough height and period) are suitable to characterize the wave associated with w_-, but they are not a direct parameter to characterize the wave associated with w_+. Some other definition of wave height and peried may provide a closer prediction of w_+. Possibilities are trough to crest height and mean of the zero upcrossing wave height and period fore and aft the zero upcrossing.

Regardless of the scattering due to the irregularity of the random wave motion, the linear regression lines are, in general, close to the relation:

$$(u_+)_{\text{observed}} = (u_+)_{\text{predicted}}, \tag{5.18}$$

i.e. $a=1.0$ and $b=0$, approximately.

5.2.3 Probability of error

The observed maximum velocities are random veriable. The predicted ones are also random variable, since they are given as the functions of two random variable: zero upcrossing wave height and period. The relative error which is defined by **Eq. (5.19)** is thus a random variable.

$$r_D = \frac{(u_+)_{\text{observed}} - (u_+)_{\text{predicted}}}{(u_+)_{\text{predicted}}}, \quad etc. \tag{5.19}$$

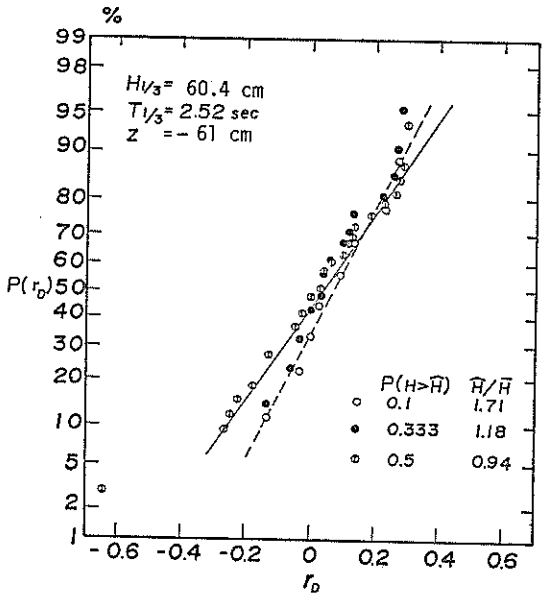

Fig. 5.7 : Probability distribution of relative error of u_+

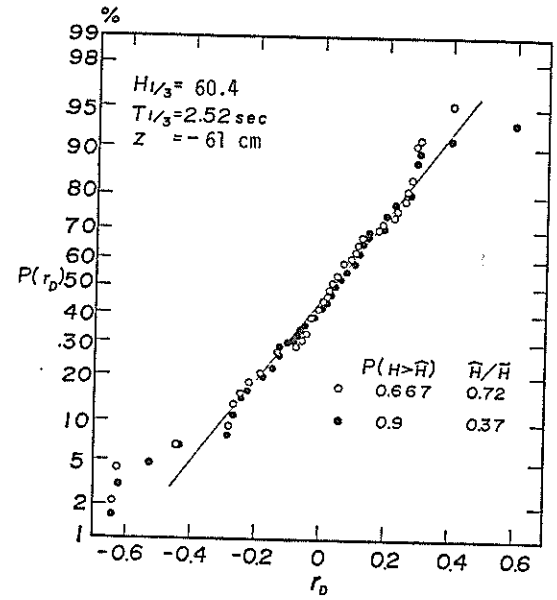

Fig. 5.8 : Probability distribution of relative error of u_+

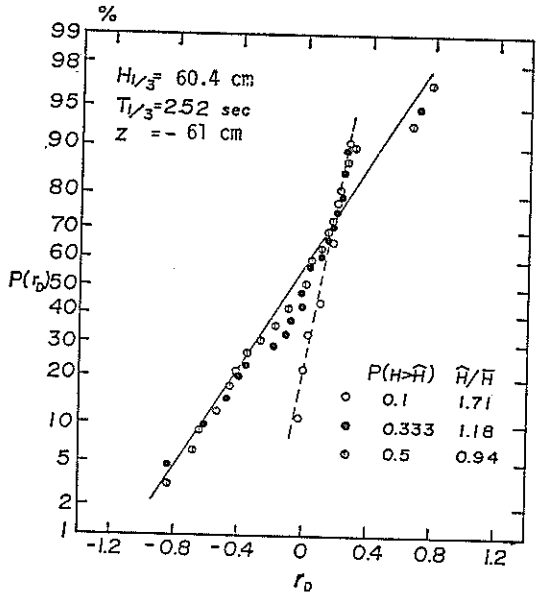

Fig. 5.9 :Probability distribution of relative error of w_+

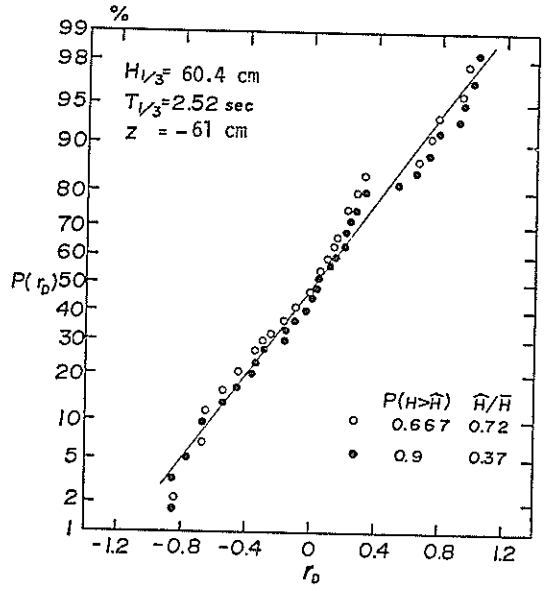

Fig. 5.10 : Probability distribution of relative error of w_+

The distribution of the relative error is plotted on a normal probabilty paper for several sample populations from a train of about 60 waves: populations of one-tenth, one-third, one-half, two-thirds and nine tenths highest waves. Some examples are shown in **Fig. 5.7** through **Fig. 5.10**. The distribution for each population is well expressed by a straight line on the normal probability paper.

The error distributions of other populations are not shown in the figures. However, almost all sample populations, except some population which include small waves, passed the Chi square test[32] at the significant level of 95% as shown in **Table 5.5**. Because of the small sample size, Chi square

tests are not done for the population of one-tenth highest waves. Thus, the distribution of the relative error is normal.

Table 5.5 Chi square test (six degree of freedom)

Spectrum	$H_{1/3}$ (cm)	$T_{1/3}$ (s)	z (cm)	Velocity	Chi sqare			
					1/3	1/2	2/3	9/10
I	84.4	2.78	−61	u_+	3.19	5.76	10.23	8.17
				u_-	3.59	5.40	4.66	8.46
				w_+	2.58	9.86	2.09	5.47
				w_-	8.08	4.00	5.97	5.69
II	60.4	2.52	−61	u_+	7.52	3.76	3.66	10.79
				u_-	2.72	4.57	5.51	8.15
				w_+	8.25	7.84	6.05	9.05
				w_-	10.76	8.67	42.11	60.46
I	84.4	2.78	−122	u_+	9.19	4.50	8.62	8.03
				u_-	5.39	4.51	5.29	7.13
				w_+	4.97	3.21	4.81	5.59
				w_-	4.96	10.40	6.10	8.84
II	60.4	2.52	−122	u_+	4.62	4.24	9.32	11.74
				u_-	8.75	8.29	20.29	28.03
				w_+	5.80	7.20	6.94	9.21
				w_-	11.28	10.89	18.97	49.09

Note : If Chi squre value is larger than 12.59, the fit is not good.

It is easily seen in **Fig. 5.7** through **Fig. 5.10** that the slopes of the distribution for one-tenth and one-third highest waves are steeper than those for others. This shows that the standard deviations of relative error for the "large wave" populations are smaller than those for the "small wave" populations. The mean and the standard deviation of the relative error for each population is summarized in **Figs. 5.11** through **5.14**, It is seen for all the cases that the standard deviations for "large wave" population are smaller than those for the population including small waves. In addition, the standard deviations for one-tenth and one-third highest waves are almost comparative to the standard deviations of the relative errors for periodic waves. (see **Table 4.5**)

Note that the design wave is a large wave.

The means of the relative errors fall within the range from −0.2 to 0.2. This range is about twice of the range observed for periodic waves (see **Table 4.5**), and the same range as seen in the statistical estimation, **Fig. 5.4**. In addition, some similar aspects of the mean relative error are observed between **Figs. 5.11** to **5.14** and **Table 4.5**. For many cases, the mean relative error for u_+ is negative while that for u_- is positive. The mean relative errors for w_+ and w_- are generally negative. This shows that the measured u_+ is smaller than the predicted u_+. On the other hand, the measured u_- is larger than the predicted one. The measured w_+ and w_- are smaller than the predicted ones. Thus, the deviation of the mean relative error from zero results from the error associated with the wave thery.

The above discussion is summarized as follows.

The mean of maxium velocities of one-tenth, one-third, etc., highest waves can be well estimated by fitting proper periodic waves to the zero upcrossing waves. The realizations of maximum velocities are normally distributed about the means, i.e. the predicted maximum velocities. The standard deviations of the relative error which is defined by **Eq.** (5.19) are small for large

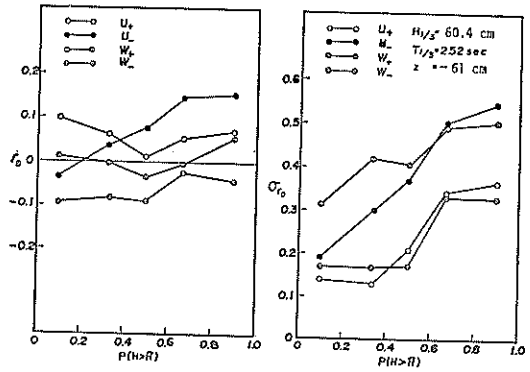

Fig. 5.11 : Mean and standard deviation of relative error (Spectrum Ⅱ, $z=-61$cm)

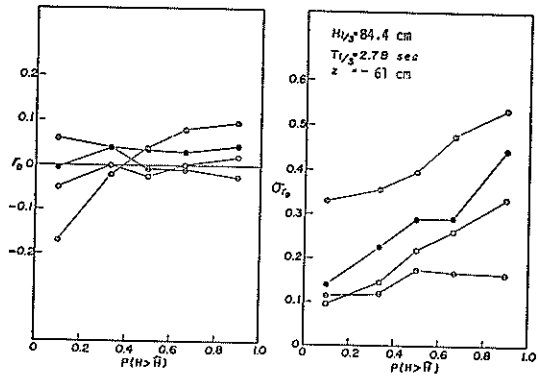

Fig. 5.12 : Mean and standard deviation of relative error (Spectrum Ⅰ, $z=-61$cm)

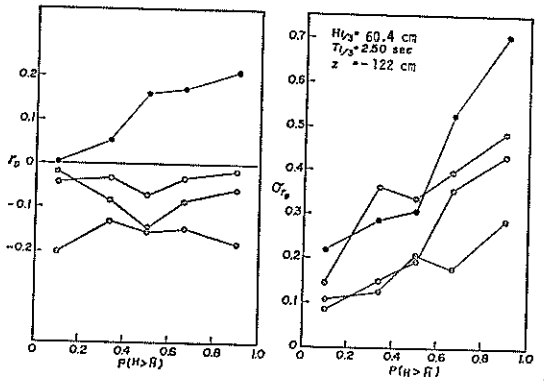

Fig. 5.13 : Mean and standard deviation of relative error (Spectrum Ⅱ, $z=-122$cm)

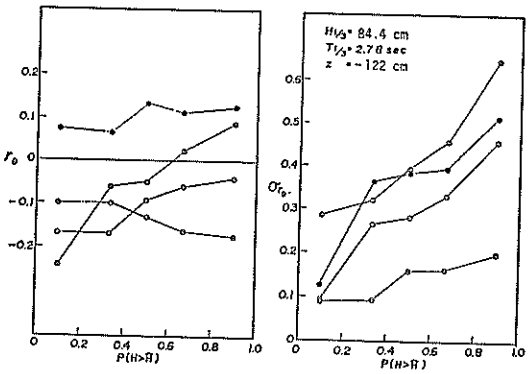

Fig. 5.14 : Mean and standard deviation of relative error (Spectrum Ⅰ, $z=-122$cm)

waves in a random wave train: the standard deviations associated with u_+, u_- are w_- are less than 0.3 for one-third highest waves, and are less than 0.2 for one-tenth highest waves.

6 Conclusions

Summing up the results of the study described above, the following are the major conclusions.

6.1 Periodic wave tests

1. The maximum horizontal and vertical velocities can be measured accurately with a hot film anemometer. The correlation between the maximum velocities measured with the hot film anemometer and those measured with the propeller current meter was quite good.

2. For deep water waves and near deep water wave conditions, i.e. h/T^2 is larger than 0.51, and within the range where H/H_b is smaller than 0.75, Stokes' fifth order theory, Dean's Stream Function Theory and Airy theory give good predictions of the maximum velocities. The mean and the standard deviation of the relative error defined by **Eq.** (4.3), turned out to be almost the same values whichever theory was used to predict the maximum velocities. This shows that Airy theory is no worse than the other two higher order wave theories for the prediction of the maximum velocities at a level below wave troughs.

3. For most cases, the magnitude of the measured horizontal velocity beneath the wave troughs are larger than those beneath the wave crests. Such a tendency detected by the stationary probe may due to the characteristics of deep water waves.

6.2 Random wave tests

1. The spectrum analyses give a good statistical estimation of the maximum velocities at a level below the wave troughs. The relative errors are less than 10 percent for most cases.

2. The maximum velocities of discrete zero upcrossing waves can be predicted by fitting appropriate periodic waves to the zero upcrossing waves. The measured maximum velocities widely scatter about the above predicted velocities. However, the relation between the measured and the predicted maximum velocities obtained by the least-squares method turned out to be close to the relation:

$$(u_+)_{\text{measured}} = (u_+)_{\text{precicted}}, \text{ etc.} \tag{6.1}$$

3. The relative errors defined by **Eq.** (5.19) are normally distributed. The characteristics of the mean relative errors are similar to the characteristics of the relative error for periodic waves. Hence, the deviation of the relative error from zero is partly caused by the error introduces by the wave theory.

4. The relative errors are smaller for "large wave" population than those for "small wave" populations.

5. Design waves are large waves. Thus, the results may make engineers confident when they use periodic wave theory to estimate the maximum velocities of the design wave.

Acknowledgement

The study presented herein was conducted in the Ocean Engineering Programs at Oregon State University, during the author's stay as a research engineer abroad. The author sincerely wishes to express his appreciation to express his appreciation to Dr. John H. Nath, Professor and Director of Environmental Fluid Dynamics Laboratory, and to Dr. Tokuo Yamamoto, Professor of Civil Engineering for their helpful advice from the planning of the experiments to the analyses of the results.

The author also wishes to express his heartfelt thanks to Dr. Nath for his critical review of the manuscript, and to Mr. Terry Dibble and Mr. Larry Crawford, Technical Staff Members of the Ocean Engineering Program for their kind assistance in the experiments.

The wave kinematics from Stokes' fifth order theory and the spectra of the test random waves were computed by the Digital Computer CYBER 71 Series at Oregon State University Computer Center. The author owes his thanks Mr. Robert Jensen, ex-graduate student in the Ocean Engineering Program, for his generous permission to use his computer program, Stokes' fifth order theory.

Reference

1) Reid, R. O., Correlation of water level variation with wave forces on a vertical pile for nonperiodic waves, *Proc. of 4th Conf. on Coastal Eng.*, 1958, pp. 749–786
2) Borgman, L. E., Ocean wave simulation for engineering design, *Proc. Conf. on Civil Eng. in the Ocean.* A. S. C. E., 1968, pp. 31–74
3) Nath, J. H. and Harleman, D. R. F., Response of vertical cylinder to random waves, Journal of the Waterways and Harbors Division, *Proc. of the A. S. C. E.*, WW2, 1970, pp. 373–386
4) Iwagaki, Y., Sakai, T. and Ishida, H., Correlation of water particle velocity with water level variation for irregular waves, *Coastal Eng. in Japan*, Vol. 16, 1973, pp. 19–28
5) Reference 1), pp. 761
6) Tsuchiya, Y. and Yamaguchi, M., Horizontal and vertical water particle velocities induced by waves, *Proc. of 14th Conf. on Coastal Eng.*, 1974, pp. 555–568

7) Grace, R. A. and Rochelean, R. T., Near-bottom velocities under Waikiki swells, *James K. K. Look Laboratory of Oceanographic Engineering*, Univ. of Hawaii, Technical Report No. 31, 1973, p. 55
8) Grace, R. A., How to measure waves:, *Ocean Industry*, Vol. 5, No. 2, 1970, pp. 65-69
9) Goda, Y., Wave forces on a vertical cylinder: Experiments and a proposed method of wave force computation, *Report of Port and Harbour Technical Research Institute*, Report No. 8, 1964, p. 74
10) Dean, R. G., Evaluation and development of water wave theories for engineering applications, U. S. *Army, Corps Engineers Coastal Engineering Research Center*, Special Report No. 1, Vol. 1, 1974, p. 121
11) LeMehaute, B., Divoky, D. and Lin. A., Shallow water waves: A comparison of theory and experiment, *Proc. of 11th Conf. on Coastal Eng.*, 1968, pp. 86-107
12) Dean, R. G., Relative validity of water wave theories, *Proc. A. S. C. E. Specialty Conf. on Civil Eng. in the Oceans*, 1968, pp. 1-30
13) Iwagaki, Y. and Sakai, T., Horizontal water particle velocity of finite amplitude waves, *Proc. 12th Conf. on Coastal Eng.*, 1970, pp. 309-325
14) Richardson, E. V. and McQuivey, R. S., Measurement of turbulence in water, Journal of the Hydraulic Division, Proc. of *A. S. C. E.*, Vol. 94, No. HY2, 1968, pp. 411-430
15) Morrow, T. B. and Kline, S. J., The evaluation and use of hot-wire and hot-film anemometer in liquids, *Thermoscience Division, Dept. of Mech. Eng. Stanford. Univ.*, Report DM-25, 1971, p. 187
16) Kato, H. and Sano, K., Characteristics of a hot-film anemometer for the measurement of turbulence in water, *Technical Note of the Port and Harbour Research Institute*, No. 157, 19 73, p. 21
17) Skjelbreia, L., Gravity waves, Stokes' third order approximation : Table of function, Council on Wave Research, The Engineering Foundation, 1959, pp. 1-337
18) Iwagaki, Y., Hyperbolic waves and their shoaling, *Proc. 11th Conf. on Coastal Eng.*, 1968, pp. 124-144
19) Kolpak, M. M. and Eagleson, P. S., A system for measuring orbital velocities in waves, *Proc. 12th Conf. on Coastal Eng.*, 1970, pp. 327-343
20) Van Dorn, W. G. and Pazan, S. E., Laboratory investigation of wave breaking, Part II: Deep water waves, Advanced Ocean Eng. Laboratory Report No. 71, *Scripps Instituttion of Oceanography*, Univ. of California, San Diego, 1975, p. 105
21) Lee, A., Grated, C. A. and Durrani, T. S., Velocities under periodic and random waves, *Proc. of 14th Conf. on Coastal Eng.*, 1974, pp. 558-574
22) Sollit, C. K. and Hurber, D. S., Large scale model testing of a submerged wave attemuation device, *Closed Loop*, MTS System Corporation, 1976, pp. 13-26
23) Reference 20), pp. 84-88
24) Dean, R. G., Evaluation and development of water wave theories for engineering application, Special Report No. 1, *U. S. Army, Corps of Engineers, Coastal Engineering Research Center*, Vol. 11, 1974, p. 534
25) Skjelbreia, L. and Hendrickson, J., Fifth order gravity wave theory, *Proc. of 7th Conf. on Coastal Eng.*, 1960, pp. 184-196
26) Ippen, A. T., *Estuary and coastline hydrodynamics*, McGraw-Hill Book Co., Inc., 1966, pp. 28
27) Bendat, J. S. and Piersol, A. G., *Random data*: Analysis and measurement procedure, Wiley-interscience a Division of John Wiley and Sons, Inc., 1971, pp. 325-326
28) Cartwright, D. E. and Longuet-Higgins, M. S., The statistical distribution of maxima of a random function, *Proc. of Royal Society* A237 (1209), 1956, pp. 212-232
29) Kinsman, B., *Wind waves*, Prentice-Hall, Inc., 1965, pp. 134
30) Hinze, J. O., *Turbulence*, McGraw-hill Book Company, 1959, pp. 103
31) Reference 27), pp. 136-137

32) Meyer, S. L., *Data analysis for scientists, and engineers*, John Wiley and Sons, Inc., 1975, pp. 355–358
33) Reference 26), pp. 156

List of symbols

a : coefficient in the linear regression relation, **Eq.** (5.17)
a_m : coefficients in Reid's numerical filter, **Eq.** (2.1)
$A(f)$: Fourier cosine transform of $\eta(t)$, **Eq.** (4.8)
$A(\theta)$: directional coefficient, **Eq.** (3.2)
b : coefficient in the linear regression relation, **Eq.**, (5.17)
b_m : coefficients in Reid's nomerical filter, **Eq.** (2.2)
$B(f)$: Fourier sine transform of $\eta(t)$, **Eq.** (4.9)
C_i : coefficients of approximating polynomial of the linearizer, **Eq.** (3.1)
E : linearized output voltage from the hot film anemometer
E_B : non-linear output voltage of the hot film anemometer
E_0 : non-linear output voltage at zero flow
$E_{1\min}$: minimum linearized output voltage (Ch. 1, Sensor 1)
$E_{2\min}$: minimum linearized output voltage (Ch. 2, Sensor 2)
$E_{1\max}$: maximum linearized output voltage (Ch. 1, Sensor 1)
$E_{2\max}$: maximum linearized output voltage (Ch. 2, Sensor 2)
f : wave frequency
$G_x(f)$: raw estimate of power spectral density
$\tilde{G}_x(f)$: smooth estimmate of power spectral density
h : water depth
H : wave height
H^2 : mean squar of zero upcrossing wave height
$\bar{H}$: mean zero upcrossing wave height
$H_{1/3}$: significant wave height
H_D : design wave height
H_p : measured wave height with pressure gauge
i : index
j : $\sqrt{-1}$
k : wave number ($k=2\pi/L$)
K : coefficient in **Eq.** (4.2)
L : wave length
L_A : wave length given by Airy theory
m : index
m_ν : νth moment of a spectrum about the origin
N : number of the record
n : frequency of the output pulses from propeller current meter (coefficient in **Eqs.** (2.15) and (2.16) in Chapter 2)
$p(x)$: probability density
$P(x)$: cumulative probability
$R_u(\omega)$: frequency response function for horizontal velocity **Eq.** (2.5)
$R_w(\omega)$: frequency response function for vertical velocity, **Eq.** (2.6)
$R'_u(f)$: frequency response function for horizontal velocity, **Eq.** (5.4)
$R'_w(f)$: frequency response function for vertical velocity, **Eq.** (5.5)
r_c : correlation coefficient
r_D : relative error of velocity estimate with periodic wave theory
$\bar{r}_D$: mean of r_D

r_p : relative error of velocity estimate for periodic waves
r_s : relative error of statistical velocity estimate
$S_{\eta\eta}(f)$: spectral density of water surface elevation
$S_H^2(\omega)$: Bretschneider spectrum
$S_{uu}(f)$: spectral density of horizontal velocity fluctuation
$S_{ww}(f)$: spectral denslty of vertical velocity fluctuation
T : wave period
$T_{1/3}$: signicant wave period
$\bar{T}$: mean zero upcrossing wave periods
T_D : design wave period
t : time
t_1, t_2 : the times when a record starts and ends, respectively
u : horizontal velocity
u_+ : horizontal velocity beneath wave crests
u_- : horizontal velocity beneath wave troughs
u_n : normal velocity component to the hot film axis, **Eq.** (4.2)
u_t : tangential velocity component to the hot film axis, **Eq.** (4.2)
V : magnitude of flow speed
v_{max} : maximum speed of the pendulum motion
w : vertical velocity
w_+ : vertical velocity when the water surface crosses the still water level upward
w_- : vertical velocity when the water surface crosses the still water level downward
$X(f)$: Fourier transform of water surface elevation, n(t)
z : vertical distance from the still water level (upward positive)
$\alpha(\theta)$: directional coefficient, **Eqs.** (2.15) and (2.16)
θ : yaw angle, the angle between flow direction and hot film sensor axis
τ : time interval
$\eta(t)$: water surface elevation
$\overline{\eta^2}$: mean square of water surface elevation
σ_{rD} : stadard deviation of r_D

Appendix A Calibration of the propeller current meter and the hot film anemometer

A.1 Calibration aparatus.

The calibration of the propeller current meter and the hot film anemometer have been usually conducted in a steady flow utilizing a water tunnel, water jet or moving carriage. However, since alternating flows due to a wave motion is of interest for the present measurement, it is desirable that the calibrations be conducted in an osillatory flow. Thus, a pendulum which could generate a damped oscillation and a carriage which was manually swayed to and fro were used.

The range of the periods of the pendulum and the carriage motion were from two seconds to three seconds. The significant wave periods of the test random waves fall into this range.

(1) Pendulum (**Fig A. 1**)

The rod is composed of aluminum tubes and iron channels. It is stiff enough so that the transverse vibration due to the Karman vortex trail is small. The displacement of the pendulum was measured utilizing the Sonic Wave Profiler. **Figure A. 2** shows the sketch of a typical record of the free damped oscillation of the pendulum.

The maximum speed at the end of the pendulum, which is used to obtain the relation of the outputs from the propeller current meter or hot film anemometer to the flow speed, is calculated as follows. A free damped oscillation of a linear system is expressed as

$$x=a_0\exp(-\zeta\omega_0 t)\cos(\sqrt{1-\zeta^2}\omega_0 t)\cdot \tag{A.1}$$

where x is the displacement of the end of the pendulum, a_0 is the initial displacement, ζ is a damping coefficient (linear assumption), ω_0 is the undamped natural frequency of the pendulm and t

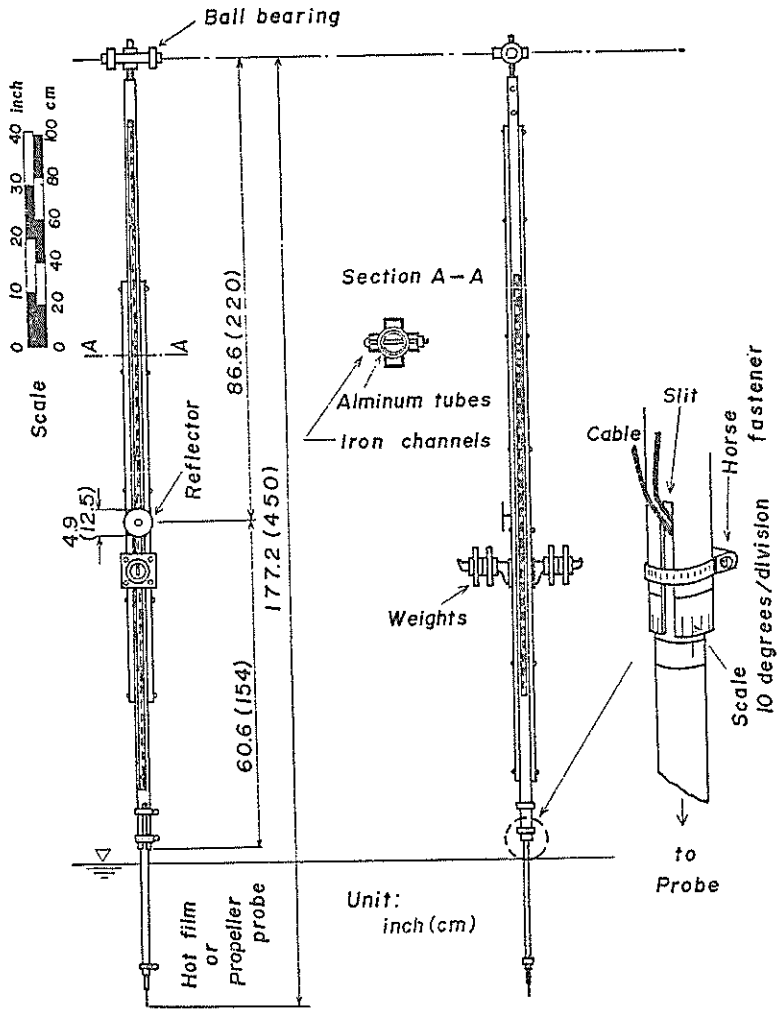

Fig. A. 1 : Pendulum

is a time.

From the record, ζ and ω_0 are calculated with the following equations.

$$\sqrt{1-\zeta^2}\ \omega_0 = 2\pi/\bar{T} \qquad \text{(A. 2)}$$

where $\bar{T} = \frac{1}{N}\sum_{i=1}^{N} T_i$

$$\exp(-\zeta\omega_0\bar{T}) = \overline{a_{1+2}/a_i} \qquad \text{(A. 3)}$$

where $$\overline{a_{i+2}/a_i} = \frac{\sum_{i=0}^{N-1}[(a_{2i+2}/a_{2i}) + (a_{2i+3}/a_{2i+1})]}{2(N-1)}$$

When the damping coefficient ζ is much smaller than 1.0, above equation can be written as

$$\omega_0 \fallingdotseq 2\pi/\bar{T}, \qquad \text{(A. 4)}$$

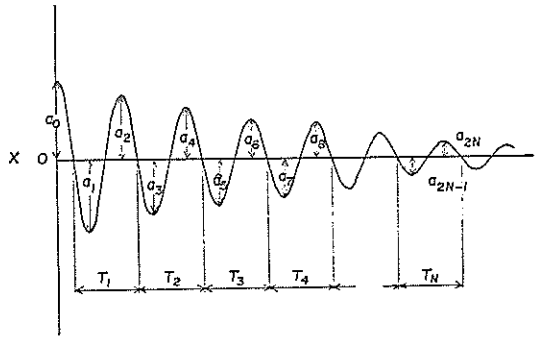

Fig. A. 2 : Sketch of a record of the pendulum motion

$$\exp(-2\pi\zeta) \fallingdotseq \overline{a_{i+1}/a_i} \tag{A. 5}$$

Now, the velocity of the pendulum, v, is obtained by differenciating **Eq.** (A. 1) with respect to time, t.

$$v \fallingdotseq a_0\omega_0 \exp(-\zeta\omega_0 t)\sin(\sqrt{1-\zeta^2}\ \omega_0 t-\phi) \tag{A. 6}$$

where $\phi=\mathrm{Tan}^{-1}\dfrac{\zeta}{\sqrt{1-\zeta^2}}$

When the damping coefficient ζ is small, ϕ is very small. For small damping coefficient, **Eq.** (A. 6) gives the amplitudes of the velocity as follows.

$$\begin{aligned}(v_{\max})_i &= a_0\omega_0 \exp\{-\zeta\omega_0\ (i+1/2)\,T/2\}\\ &= a_0\omega_0 \exp\{-\zeta\omega_0 iT/2\}\exp(-\zeta\omega_0 T/4)\\ &\qquad i=0, 1, 2, \cdots\cdots, N\end{aligned} \tag{A. 7}$$

On the other hand, the amplitude of the displacement is obtained from **Eq.** (A. 1) as

$$a_i = a_0 \exp\{-\zeta\omega_0 iT/2\}, \tag{A. 8}$$

$$\begin{aligned}a_{i+1} &= a_0\exp\{-\zeta\omega_0(i+1)T/2\}\\ &= a_0 \exp\{-\zeta\omega_0 iT/2\}\ \exp(-\zeta\omega_0 T/2).\end{aligned} \tag{A. 9}$$

The function $\exp(-y)$ is expressed in the Taylor expansion.

$$\exp(-y) = 1-y+\frac{1}{2}y^2-\frac{1}{6}y^3+\cdots\cdots \tag{A. 10}$$

Hence, for small damping coefficient ζ, **Eq.** (A. 7) and **Eq.** (A. 9) can be approximated as follows.

$$(v_{\max})_i = a_0\omega_0 \exp\{-\zeta\omega_0 iT/2\}\ (1-\zeta\omega_0 T/4) \tag{A. 11}$$

$$a_{i+1} = a_0 \exp\{-\zeta\omega_0 iT/2\}\ (1-\zeta\omega_0 T/2) \tag{A. 12}$$

From **Eqs.** (A. 8). (A. 11) and (A. 12), i. e. maximum velocity is expressed in terms of the amplitudes of the pendulum displacement.

$$(v_{\max})_i = \omega_0\frac{a_i+a_{i+1}}{2},\quad at\ t=(i+\frac{1}{2})\frac{T}{2} \tag{A. 13}$$

Thus the maximum velocities are theoretically calculated from the displacement records. They are compared with the output from the propeller current meter and the hot film anemometer.

(2) Carriage (**Fig. A. 3**)

A T-shaped carriage was also used to calibrate the propeller current meter. Since the carriage was manually driven, the motion was no longer sinusoidal. So, the speed of the carriage was calcuated as the slope of the displacement record which was measured with a pair of the Sonic Wave Profilers.

$$v=\frac{\Delta x}{\Delta t} \tag{A. 14}$$

where Δt is a time interval and Δx the displacement of the carriage in the time interval Δt.

The above calculated speed was compared with the output from the propeller current meter in the calibration.

A. 2 Calibrtation

(1) Propeller current meter

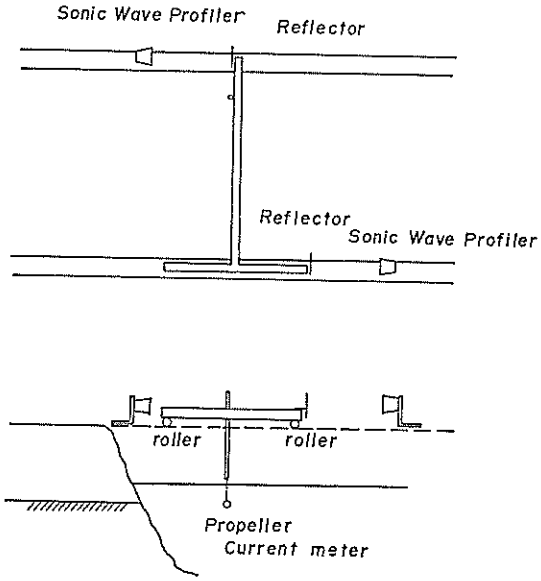

Fig. A. 3 : T-shape carriage

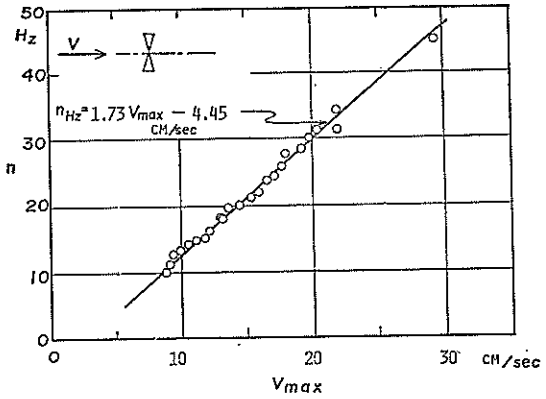

Fig. A. 4 : Calibration of propeller current meter for low speed range

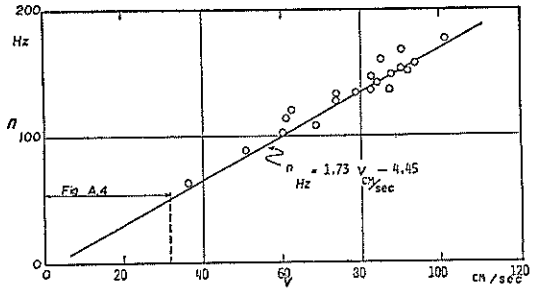

Fig. A. 5 : Calibration of propeller current meter for high sperd range with T-shape carriage

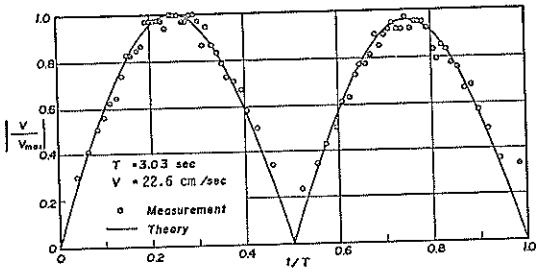

Fig. A. 6 : Response of propeller

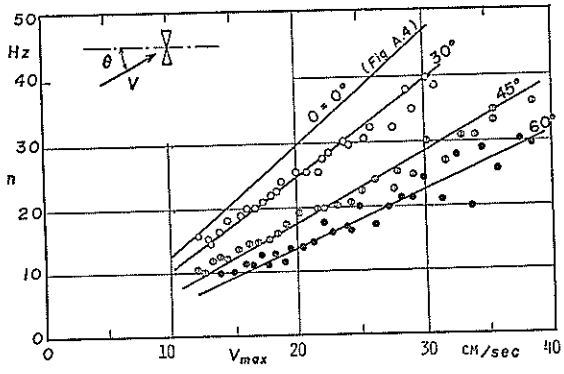

Fig. A. 7 : Effect of flow direction on propeller response

As mentioned in **Chapter 3**, the output from the propellerer current meter is the pulses which are generated by the passage of the blades past the gold tip within the head of the support. **Figure A. 4** shows the relation of the maximum frequencies of the pulses to the maximum speeds calculated from **Eq.** (A. 13), during one trial of the damped oscillation of the pendulum. The relation is well approximated by a straight line, **Eq.** (A. 15).

$$n=1.73\ v_{max}-4.45 \qquad \text{(A. 15)}$$

where n is the frequency of the output pulses (Hz), i. e. $n=1/\Delta t$, Δt is the time interval between two adjacent pulses and v_{max} is the maximum speed of the pendulum (cm/s). The line given by above equation fits the frequency-maximum speed correlation in high speed range (**Fig.** A. 5) which was tested utilizing the T-shape carriage.

Having obtained the relation of the pulse frequency to the flow speed, one can reduce the output pulses to flow speed at any stage during one cycle of the pendulum oscillation. The measured time variation of the flow speed is compared with theoretical variation, **Eq.** (A. 16) in **Fig. A. 6**

$$\left|\frac{v}{v_{max}}\right|=\left|\frac{\exp(-\zeta\omega_0 t)\ \sin(\sqrt{1-\zeta^2}\,\omega_0 t)}{\exp(-\zeta\omega_0 T/4)}\right|,\quad 0<t<T. \qquad \text{(A. 16)}$$

Though the observed variation is not smooth due to the accuracy of record reading, it agrees quite well with the theoretical variation. Some differences of the measured speed from the theoretical variation are seen in the low speed range. This is because the relation, **Eq.** (A. 15), can not hold

such a range. Thus it can be said that the propeller has good response to oscillating flow within the frequencies tested.

The flow in waves changes its mangitude and direction, and it is generally expressed by the horizontal and vertical components. It is thus desirable that the propeller responds only to the velocity component which direction is parallel to the propeller spindle. The angular response was tested utilizing the pendulum and twisting the propeller probe by θ=30, 45 and 60 degrees. The angle was measured with the scale marked on the aluminum tube (see **Fig A. 1**), so the ambiguity of the angle was ±5 degrees.

The results are plotted in **Fig. A. 7.** The relation between the maximum frequency of the pulses and the flow speed for each propeller angle can be expressed by a staight line. The slpoe the the line decreases according to the increase of the angle, θ. The change of the the propeller response due to the angle is clearly shown in **Fig. A. 8.** The dots in the figure show the relation given by the straight lines for respective angles in **Fig. A. 7,** and they agree with the curve given by **Eq.** (A. 17).

$$n=1.73\ v_{max}\cos\theta-4.45 \qquad \text{(A. 17)}$$

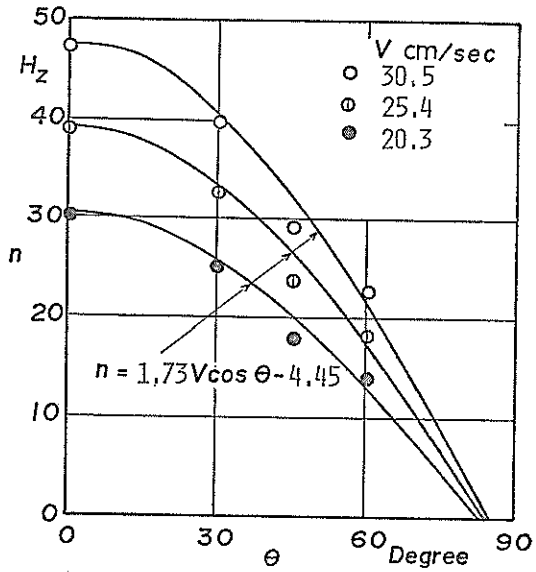

Fig. A. 8 : Angular sensitivity of propeller

(2) Hot film anemometer

All the calibrations of the hot fim anemometer were conducted utilizing the pendulum. A typical record of the linearized output from Sensor 1 (outer sensor) is shown in **Fig. A. 9,** and that of Sensor 2 (inner sensor)is shown in **Fig. A. 10.** In these figures, theoretical curve of the damped free oscillation given by **Eq.** (A. 18) is plotted with dotted line.

$$E=E_{max,0}\exp(-\zeta\omega_0 t)\ \sin(\sqrt{1-\zeta^2}\omega_0 t)/\exp(-\zeta\omega_0 T/4) \qquad \text{(A. 18)}$$

where $E_{max,0}$ is defined as show in the figures, ζ and ω_0 are calcurated from **Eq.** (A. 5) and **Eq.** (A. 4)

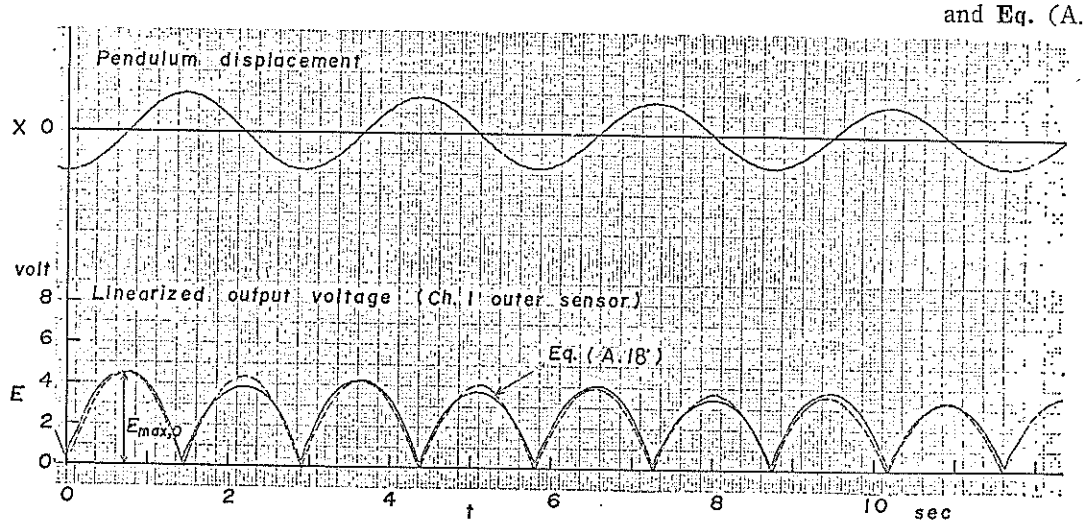

Fig. A. 9 : Response of hot film anemometer to an oscillatory flow (Sensor 1)

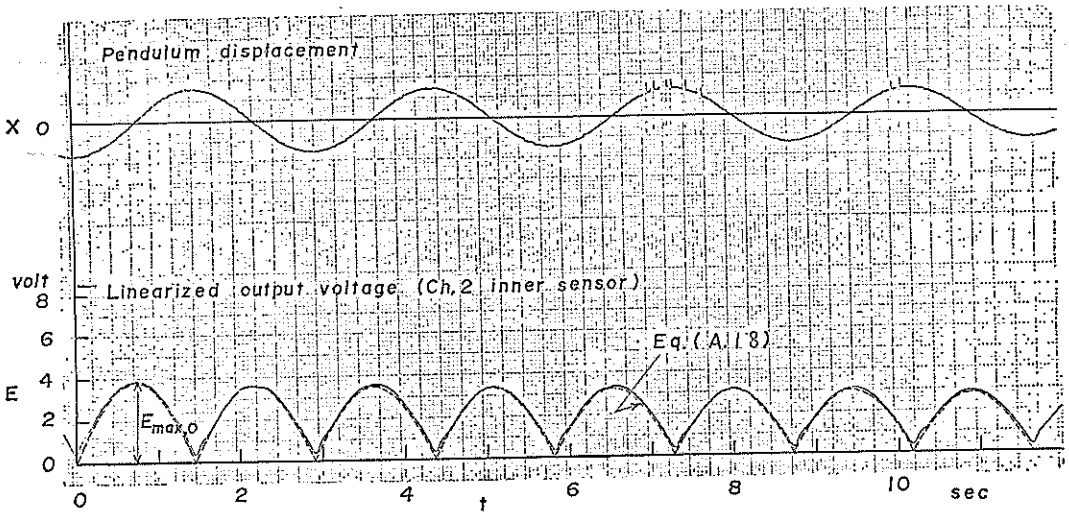

Fig. A. 10 : Response of hot film anemometer to an oscillatory flow (Sensor 2)

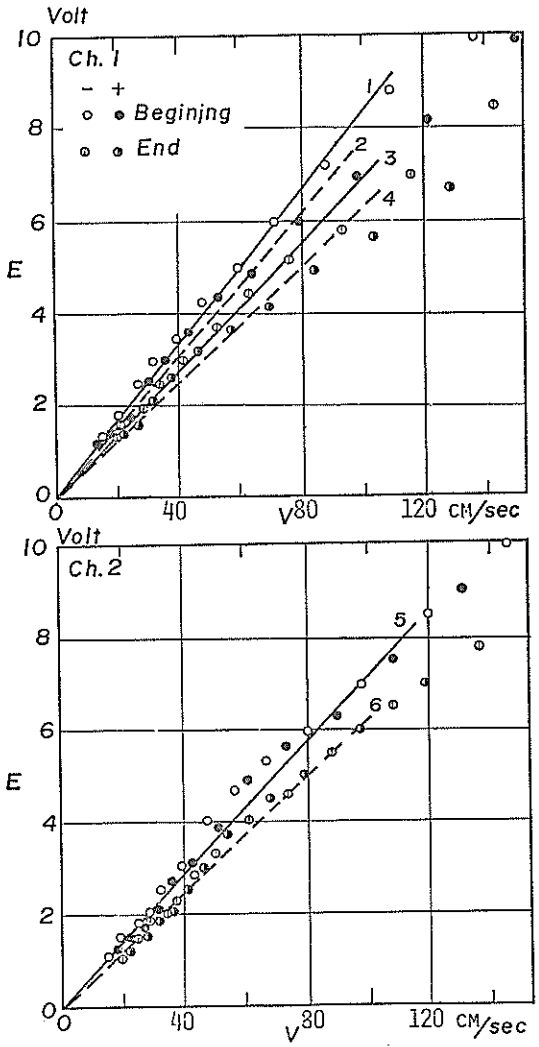

Fig. A. 11 : Calibration for periodic wave tests (Series I)

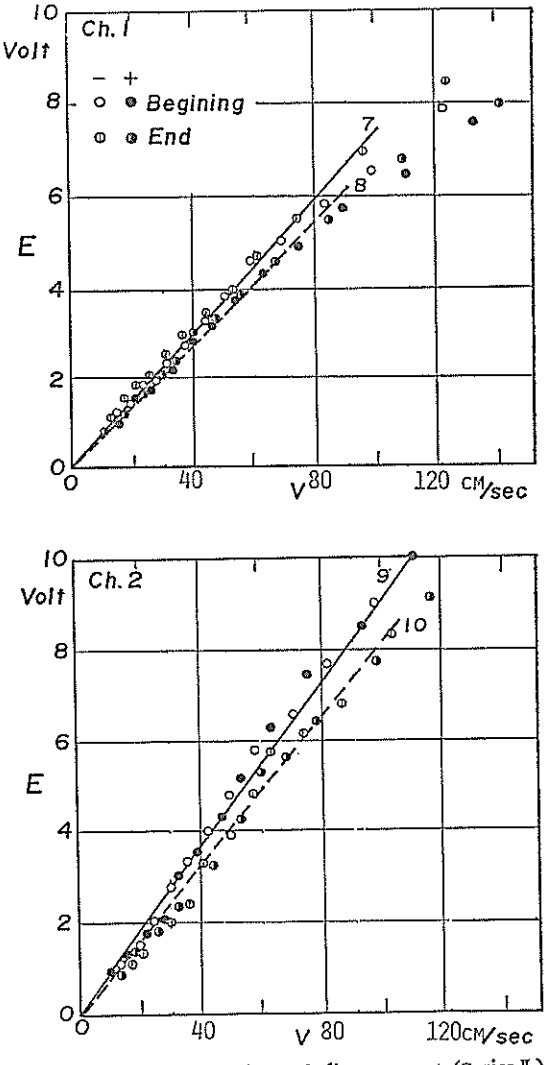

Fig. A. 12 : Calibration for periodic wave tests (Series II)

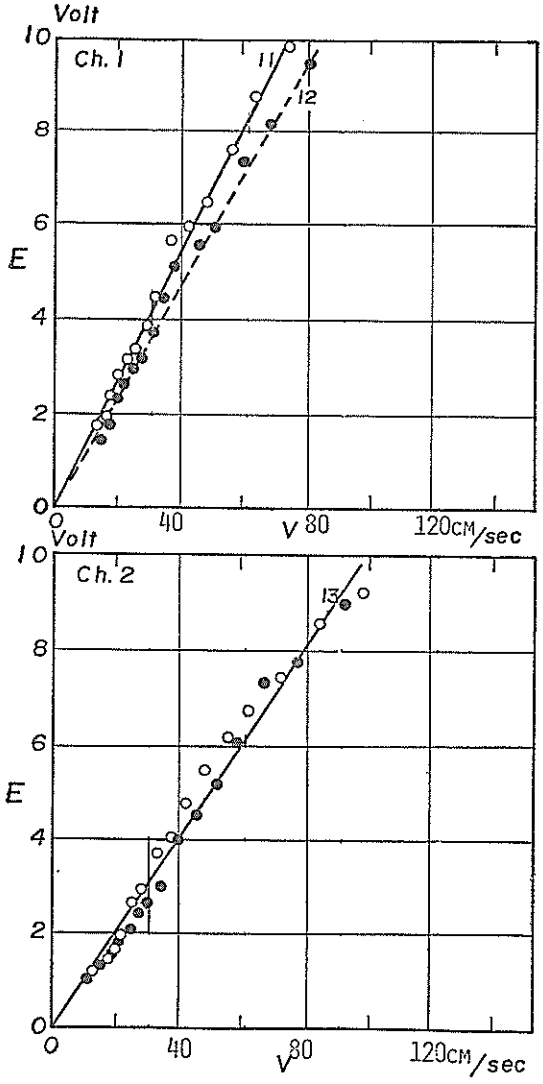

Fig. A. 13 : Calibration for random wave tests
($z=-61$cm)

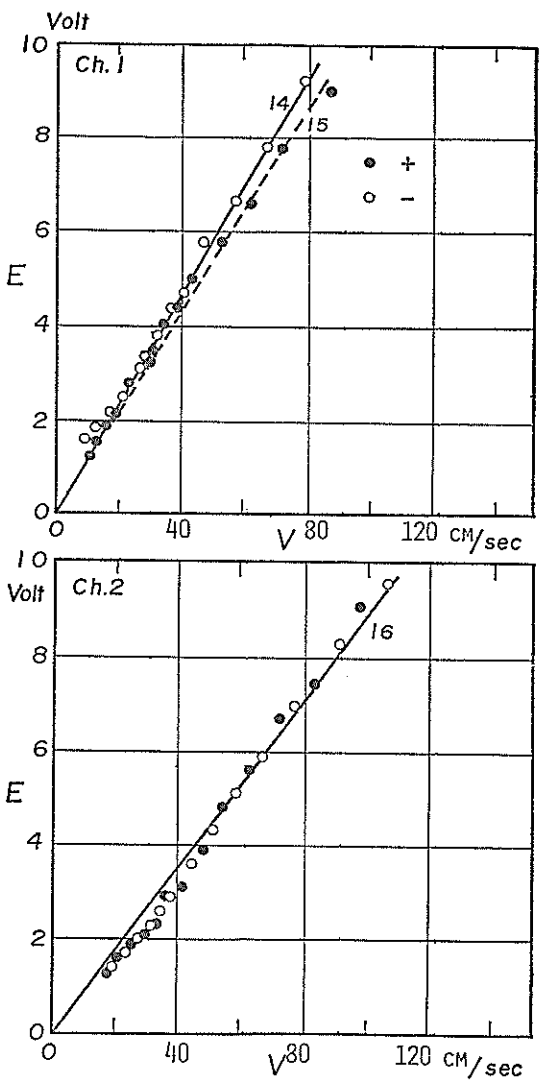

Fig. A. 14 : Calibration for random wave tests
($z=-122$cm)

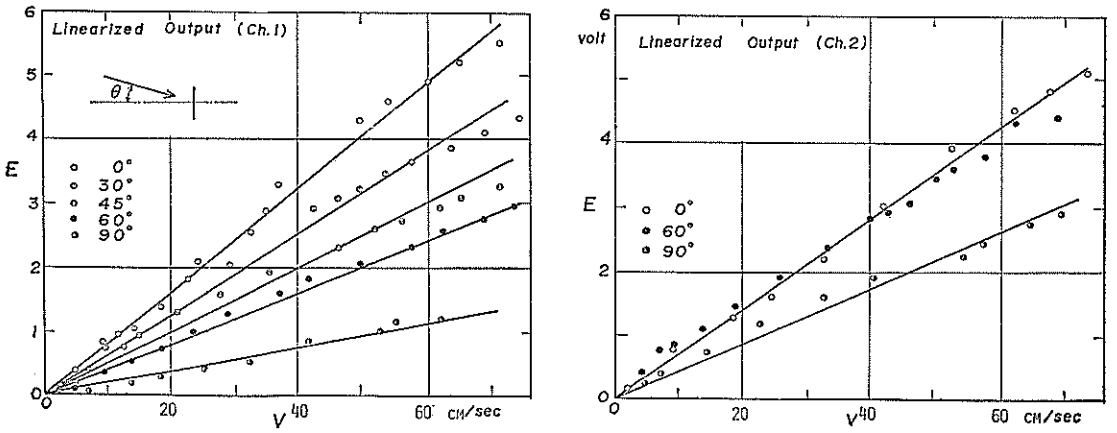

Fig. A. 15 : Angular sensitivity of hot film sensors

respectively. For this case, the damping coefficients ζ is 0.0133 and ω_0 is 2.161 radian per second. very other peak of the linearized output from the outer sensor is smaller than that of the theoretical curve (**Fig. A. 9**). On the other hand vaiation of the output from the inner sensor is very close to the theortical one (**Fig. A. 10**). This shows the response characteristics of the outer sensor the flow of one direction is different from that to the flow of opposite direction.

Taking such characteristics of the outer sensor into accout, it can be said that the agreement of these two curves is fairly good and that the linearizers functioned well.

It is well known that the relation between fluid speed and output voltage from a hot film anemometer is easily affected by dirt and fluid temperature change. Therefore, the hot film anemometer was calibrated at the begining and the end of each series of runs. The first half runs were processed using the result of the calibration at the begining while the latter half runs were processed using that at the end.

Figures. A. 11 through **A. 14** show the relations of the maximum output voltage to the maximum speed, **Eq.** (A. 13), obtained from the calibrations. The slope of the calibration curve decrease after a series of runs due to the dirt and the temperature change. The relations given by these curves are listed in **Table 4. 1** and **Table 4. 6** (**Chapeter 4**).

The angular sensitivity of each sensor was examined in the same way as the propeller probe was tested. **Figres A. 15** and **A. 16** show the results for the outer (Ch. 1) and the inner sensor (Ch. 2) respectively. The difference between the angular sensivity of these two sensor is obvious: the outer sensor is very sensitive to the angle θ while the inner sensor shows same E—v relation over the range $\theta<60$ degree*. Thus the angular sensitivity of a hot film sensor varies from sensor to sensor.

Appendix B Experimental data in random waves

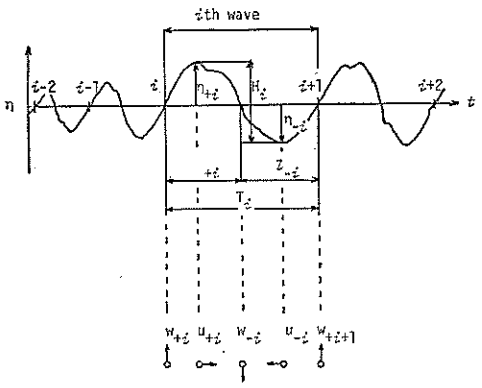

Definition Scketch

Unit: η_+, η_-, H cm
τ_+, τ_-, T sec
u_+, u_-, w_+, w_- cm / sec

* The test for another probe yielded opposite result: the outer sernsor did not have any angular sensitivity over the range $\theta<45°$, while the inner sensor showed remarkable angular sensitivity as **Fig. A. 15.**

(1) Series III, Run 1, Spectrum I, z = -61 cm

No.	η_+	η_-	z_+	z_-	H	T	Hot film u_+	Hot film u_-	Hot film w_+	Hot film w_-	Propeller u_+	Propeller u_-	Propeller w_+	Propeller w_-
1	24.6	31.9			56.5	3.47	46.0	66.8	20.1	39.0	36.6	70.9	22.5	36.6
2	52.6	44.4			96.9	2.91	78.9	89.0	64.6	86.0	70.7	82.0	62.2	69.9
3	32.8	10.5			43.3	2.25	57.0	18.9	74.7	30.2	55.6	21.3	69.8	25.4
4	6.6	1.7			8.2	1.50	9.1	—	16.8	4.6	11.4	—	17.0	—
5	3.9	13.1			17.1	2.30	11.0	26.5	6.7	16.8	—	28.4	—	14.6
6	29.6	30.9			60.4	3.10	46.9	61.6	34.4	50.3	44.0	60.1	34.7	55.6
7	23.7	18.7			42.4	2.86	37.5	36.0	51.2	29.0	37.9	32.4	38.7	35.5
8	16.4	13.8			30.2	1.92	26.5	25.6	34.4	24.7	26.4	27.0	33.0	26.4
9	3.3	6.3			9.5	1.03	4.6	3.4	10.1	4.6	—	—	12.5	—
10	26.3	21.0			47.3	2.25	48.8	51.5	22.3	42.4	44.0	48.0	24.8	43.9
11	11.5	4.6			16.1	1.36	25.6	6.7	33.5	15.5	29.1	—	33.0	23.8
12	20.4	19.7			40.1	3.89	40.2	37.8	15.5	20.1	40.7	37.9	19.1	24.8
13	67.3	46.0			113.3	3.05	82.6	78.9	69.2	78.0	75.9	82.0	60.4	81.8
14	65.7	41.1			106.7	2.91	79.6	69.5	83.5	89.3	82.0	66.1	81.8	88.9
15	13.1	17.1			30.2	4.36	16.5	32.6	35.7	15.5	15.1	29.1	36.6	17.8
16	17.4	18.1			35.5	3.24	31.1	43.0	18.0	23.5	35.5	48.0	23.2	30.6
17	19.7	11.5			31.2	2.06	38.4	25.6	31.1	26.8	37.9	29.8	28.4	27.7
18	32.8	41.4			74.2	2.20	36.6	79.6	33.5	78.0	39.3	82.0	35.5	75.9
19	57.5	39.8			97.2	2.86	80.8	77.1	88.1	75.9	82.0	75.9	70.7	82.0
20	29.6	34.5			64.0	3.19	60.7	75.3	64.6	42.4	62.2	70.7	58.7	42.3
21	44.4	7.6			51.9	3.14	64.3	11.9	71.3	15.5	62.2	15.8	62.2	25.8
22	21.3	23.0			44.4	2.30	40.2	46.3	18.0	42.4	42.3	44.0	23.8	44.0
23	34.5	19.7			54.2	2.25	54.3	43.0	55.8	36.9	47.6	44.0	50.3	27.7
24	11.5	29.6			41.4	4.46	14.6	45.4	20.1	26.8	16.2	50.3	31.5	36.6
25	59.1	19.7			78.3	2.53	63.4	34.1	68.9	53.6	50.3	37.9	66.1	55.6
26	3.3	2.6			5.9	1.59	7.3	8.5	16.8	8.8	—	—	14.1	—
27	8.2	4.9			13.1	1.55	12.8	6.7	12.2	8.8	22.4	—	—	—
28	13.5	18.4			31.9	2.06	22.0	52.1	11.3	28.0	22.9	52.8	12.6	31.5
29	35.5	14.8			50.2	1.55	48.8	24.7	45.7	30.2	44.0	23.8	36.6	31.5
30	26.3	30.2			56.5	2.67	39.3	65.8	39.0	44.5	35.5	62.2	35.5	52.8
31	48.3	30.9			79.2	3.52	70.7	58.2	67.1	61.3	70.7	58.7	75.9	62.2
32	64.0	46.0			110.0	3.10	75.3	80.5	20.1	80.5	70.7	75.9	21.6	89.3
33	22.3	32.8			55.2	4.08	33.8	61.6	53.6	20.1	35.5	66.1	52.8	27.7
34	47.0	36.1			83.1	2.72	77.1	82.3	71.3	79.3	70.7	75.9	58.7	75.9
35	26.3	15.8			42.0	3.19	44.8	18.9	67.1	32.3	42.3	25.8	66.1	35.5
36	16.4	9.9			26.3	1.92	25.6	—	23.5	20.1	26.4	—	24.2	13.2
37	6.6	21.3			27.9	2.39	11.9	44.5	13.4	15.5	—	40.7	12.9	12.8
38	52.6	39.4			92.0	2.67	81.7	94.2	60.4	83.8	82.0	97.9	55.6	82.0
39	29.6	11.5			41.1	2.49	60.7	13.7	71.3	26.8	62.2	14.4	62.2	27.7
40	1.6	8.9			10.5	2.06	7.3	15.5	12.2	7.9	—	12.2	13.5	6.4
41	18.1	24.6			42.7	2.39	27.7	43.0	15.5	39.0	42.3	50.3	18.7	44.0
42	37.8	23.0			60.8	1.83	52.4	38.4	46.9	44.5	48.0	37.9	48.0	50.3
43	37.8	31.2			69.0	2.44	51.5	65.2	51.2	60.4	50.3	70.7	52.8	66.1
44	21.3	3.3			24.6	1.45	36.6	8.5	41.2	12.2	42.3	—	55.6	14.5
45	12.5	32.8			45.3	2.49	21.0	58.2	13.4	44.5	20.2	58.7	13.3	48.0
46	41.1	30.5			71.6	2.30	69.8	70.1	67.1	57.9	70.7	70.7	70.7	62.2
47	33.8	23.7			57.5	2.44	66.1	54.0	63.7	52.4	66.1	58.7	62.2	50.3
48	16.4	4.9			21.3	2.49	31.1	4.3	31.1	13.4	39.3	—	33.3	15.8
49	1.6	24.6			26.3	1.92	16.5	58.8	10.1	22.3	—	58.7	—	22.4
50	67.3	49.3			116.6	2.30	92.7	97.5	65.8	89.3	89.3	97.9	58.7	89.2

(1) Series III, Run 1, Spectrum I, z = -61 cm (continued)

No.	η_+	η_-	ζ_+	ζ_-	H	T	Hot film u_+	Hot film u_-	Hot film w_+	Hot film w_-	Propeller u_+	Propeller u_-	Propeller w_+	Propeller w_-
51	43.3	33.5			76.8	3.05	82.6	72.9	80.5	55.8	82.0	70.7	82.0	58.7
52	25.0	18.1			43.0	3.24	44.8	34.1	52.4	25.6	42.3	36.6	55.6	29.1
53	18.1	14.8			32.8	2.72	36.6	19.8	33.5	21.3	39.3	18.2	32.4	28.4
54	8.2	4.9			13.2	1.64	6.4	3.4	15.5	7.9	—	—	21.3	—
55	21.3	36.5			57.8	3.00	39.3	73.8	14.6	53.6	42.3	75.9	14.5	52.8
56	54.5	20.7			75.2	3.66	71.6	35.1	81.4	42.4	70.7	34.4	82.0	45.9
57	32.2	36.1			68.3	2.25	66.1	86.6	22.3	67.1	66.1	89.3	23.8	66.1
58	31.2	17.7			48.9	2.35	54.3	29.9	65.8	32.3	55.6	28.4	66.1	36.6
59	23.0	19.7			42.7	2.44	33.8	36.9	35.7	32.3	35.5	34.4	36.6	31.5
60	37.8	31.2			69.0	2.55	68.9	71.9	44.5	57.9	66.1	70.7	45.9	56.4
61	39.4	41.1			80.5	3.28	73.5	96.0	65.8	62.5	70.7	88.9	62.2	66.1
62	55.8	46.0			101.8	2.91	88.1	98.5	73.8	83.8	82.0	97.9	70.7	89.3
63	39.4	31.2			70.6	2.81	66.1	58.2	77.1	50.3	66.1	52.8	75.9	52.8
64	31.2	26.3			57.5	2.53	44.8	54.9	53.6	44.5	39.3	55.6	58.7	48.0
65	26.3	20.0			46.3	2.20	46.0	36.9	62.5	35.7	40.7	42.3	55.6	37.4
66	17.1	16.6			30.9	2.20	32.0	24.1	31.1	29.0	36.6	25.3	35.5	29.1

(2) Series III, Run 2, Spectrum II, z = -61 cm

No.	η_+	η_-	ζ_+	ζ_-	H	T	Hot film u_+	Hot film u_-	Hot film w_+	Hot film w_-	Propeller u_+	Propeller u_-	Propeller w_+	Propeller w_-
1	8.2	6.7	1.41	1.69	14.9	3.1	11.0	15.5	10.1	11.3	21.1	24.6	9.3	10.0
2	5.8	12.5	2.81	1.41	12.3	4.2	7.3	25.6	8.8	11.3	16.6	36.5	8.4	14.7
3	29.6	29.6	1.31	1.31	59.1	2.6	47.9	68.6	31.1	50.3	42.6	59.0	29.2	48.0
4	37.8	22.9	1.03	1.03	60.7	2.1	55.2	56.4	62.5	50.3	47.1	46.0	64.3	48.9
5	24.7	8.2	1.31	1.69	32.9	3.0	34.8	11.3	49.1	20.1	33.4	18.5	44.7	20.4
6	9.8	4.6	1.69	1.13	14.3	2.8	14.6	12.8	11.3	8.8	13.1	11.3	12.6	9.4
7	5.5	6.7	0.94	1.03	12.2	2.0	10.1	17.1	8.8	8.8	10.3	18.0	7.7	12.2
8	23.8	22.9	1.22	1.22	46.6	2.4	34.8	54.9	20.1	39.0	31.5	48.9	25.7	40.5
9	24.7	10.1	1.13	0.94	34.8	2.1	38.4	27.4	49.1	24.7	33.4	23.6	41.8	26.9
10	11.6	4.9	0.94	1.31	16.5	2.3	15.5	8.5	16.8	11.3	15.1	8.2	19.1	11.0
11	13.1	13.4	0.44	0.61	26.5	1.1	22.9	40.0	11.3	24.7	23.6	33.4	9.9	23.6
12	12.8	12.8	1.83	1.17	25.6	3.0	20.1	30.8	24.7	13.4	19.1	33.4	21.1	18.0
13	18.9	14.6	1.13	0.70	33.5	1.8	28.4	40.2	24.7	31.1	33.4	38.2	24.6	35.6
14	29.0	23.8	0.89	1.31	52.7	2.2	42.1	51.5	36.9	35.7	41.2	46.7	38.2	41.2
15	38.7	25.6	1.22	1.59	64.3	2.8	62.2	54.9	50.3	49.1	54.0	44.7	48.9	54.0
16	21.3	13.7	1.50	1.59	35.1	3.1	38.4	36.9	26.8	24.7	33.4	31.5	26.9	22.7
17	35.1	18.9	1.17	1.64	54.0	2.8	51.5	46.3	23.5	41.2	41.2	31.5	26.9	41.2
18	28.0	7.0	1.41	0.75	35.1	2.2	35.7	10.4	31.1	18.0	35.6	11.0	33.4	25.7
19	5.8	27.1	0.56	1.31	32.9	1.9	15.5	71.0	8.8	26.8	15.1	55.0	7.9	33.4
20	57.6	36.3	1.17	1.78	93.9	3.0	82.6	81.4	73.8	67.1	74.9	73.8	60.4	60.4
21	39.3	29.6	1.31	1.64	68.9	3.0	65.2	56.4	62.5	47.9	60.4	52.9	54.0	47.1
22	42.7	26.2	1.27	1.50	68.9	2.8	57.0	51.5	60.4	51.2	48.9	54.0	54.0	48.9
23	24.7	24.7	1.59	0.98	49.4	2.6	36.6	51.5	36.9	47.9	33.4	44.7	31.5	48.9
24	9.1	3.4	0.75	0.84	12.5	1.6	21.0	12.8	36.9	7.9	12.9	12 0	28.3	4.2
25	13.1	13.3	1.22	0.98	26.2	2.2	24.7	22.3	14.6	18.9	23.6	21.1	11.8	21.1
26	16.5	26.2	1.08	1.22	42.7	2.3	26.5	56.4	26.8	35.7	28.3	52.9	23.6	35.6
27	40.5	24.1	1.08	1.74	64.6	2.8	71.6	64.3	61.3	49.1	65.1	60.4	52.9	44.7

(2) Series III, Run 2, Spectrum II, z = -61 cm (continued)

No.	η_+	η_-	ζ_+	ζ_-	H	T	Hot film				Propeller			
							u_+	u_-	w_+	w_-	u_+	u_-	w_+	w_-
28	18.0	11.6	1.31	2.06	29.6	3.4	47.9	18.9	35.7	20.1	38.2	21.9	34.5	19.7
29	21.3	18.9	0.94	1.13	40.2	2.1	44.8	30.8	22.3	35.7	36.4	30.8	24.6	31.5
30	13.1	22.9	1.41	1.13	36.0	2.5	23.8	38.4	24.7	33.5	23.6	33.4	23.6	30.3
31	13.1	4.0	1.03	0.84	17.1	1.9	22.0	6.7	40.2	13.4	16.6	—	41.2	15.4
32	6.7	11.6	0.70	1.13	18.3	1.8	11.0	30.8	10.1	13.4	10.2	21.9	7.0	15.1
33	10.4	7.6	0.89	0.70	18.0	1.6	14.6	7.6	13.4	11.3	14.2	—	17.5	12.9
34	9.8	29.0	1.50	1.22	38.7	2.7	11.9	63.4	13.4	30.2	12.2	63.9	11.7	40.5
35	41.2	3.7	1.08	0.70	44.8	1.8	47.9	7.7	64.6	20.1	42.5	—	57.7	21.9
36	0.3	13.1	0.42	1.55	13.4	2.0	3.7	23.2	4.6	6.7	—	25.7	—	14.4
37	13.1	1.5	1.50	0.38	14.6	1.9	23.8	—	20.1	—	23.6	—	17.0	8.8
38	3.4	26.2	0.66	1.55	29.6	3.2	9.5	60.1	3.4	18.9	9.7	61.9	—	33.4
39	54.3	16.5	0.98	2.06	70.7	3.0	77.1	40.2	67.1	35.7	72.7	33.4	63.5	34.5
40	13.1	19.8	2.20	1.41	32.9	3.6	30.2	47.9	8.8	37.8	25.7	39.3	12.9	29.0
41	18.0	3.4	1.22	0.38	21.3	1.6	36.6	4.3	40.2	18.9	35.6	—	35.6	12.6
42	8.5	16.5	0.70	1.08	25.0	1.8	14.6	36.9	4.6	28.0	36.9	28.3	—	25.7
43	13.4	13.1	1.36	1.13	26.5	2.5	32.0	25.6	29.0	21.3	25.7	17.0	26.9	22.7
44	9.8	8.2	1.22	1.74	18.0	3.0	17.4	12.8	21.3	15.5	8.5	—	18.0	14.8
45	5.2	6.1	0.84	0.94	11.3	1.8	—	8.5	—	8.8	—	16.2	—	11.7
46	37.8	22.9	0.75	1.13	60.7	1.9	49.7	55.8	16.8	42.4	44.7	43.2	23.6	44.7
47	13.1	16.5	1.55	1.13	29.6	2.7	30.2	30.8	41.2	20.1	28.3	34.5	31.5	24.6
48	22.9	14.0	1.03	1.22	36.9	2.3	34.8	27.4	37.8	25.6	25.7	24.6	36.9	25.7
49	6.7	6.7	1.17	0.94	13.4	2.1	16.5	15.5	11.3	13.4	15.8	18.0	14.8	11.3
50	18.9	18.6	0.84	0.94	37.5	1.8	22.9	10.4	18.0	31.1	19.1	33.4	19.7	38.2
51	22.9	21.3	1.41	1.22	44.2	2.6	39.3	49.7	40.2	33.5	33.4	41.2	39.6	33.4
52	13.1	25.6	2.20	1.22	38.7	3.4	24.7	57.3	30.2	28.0	20.4	54.0	28.3	31.5
53	6.7	3.7	0.52	0.38	10.4	0.9	9.1	—	20.1	—	—	—	23.6	—
54	32.9	31.6	1.22	1.31	69.5	2.5	51.5	79.6	33.5	64.6	42.8	74.9	28.3	61.9
55	41.2	11.6	1.13	1.31	52.7	2.4	57.0	24.1	76.0	36.9	54.0	24.6	60.4	31.5
56	6.7	7.3	1.97	0.84	14.0	2.8	11.0	13.7	13.4	13.4	10.8	14.4	12.0	12.6
57	14.6	19.5	1.22	1.13	34.1	2.4	21.0	36.9	20.1	26.8	19.7	28.3	18.9	27.6
58	14.6	20.4	1.88	1.55	35.1	3.4	24.7	58.2	31.1	21.3	18.0	48.9	25.7	29.0
59	40.8	24.7	1.08	1.31	65.5	2.4	68.9	53.0	54.6	36.9	54.0	57.0	44.7	42.8
60	32.9	29.0	1.22	1.22	61.9	2.4	55.2	53.0	53.6	53.6	48.9	48.9	44.7	55.2
61	54.3	29.0	1.27	1.69	83.2	3.0	71.6	55.8	72.5	60.4			68.7	60.4
62	18.0	10.1	1.50	2.02	28.0	3.5	25.6	16.2	36.9	16.8			31.5	23.6
63	16.8	18.0	1.13	1.22	34.8	2.4	28.4	31.7	13.4	22.3			19.1	28.3
64	28.0	21.3	0.94	1.03	49.4	2.0	42.1	51.5	36.9	37.8			35.6	39.6
65	15.9	8.2	0.94	0.84	24.1	1.8	22.9	19.8	39.0	13.4			34.5	16.6
66	9.8	7.0	0.66	1.13	16.8	1.8	11.9	14.6	13.4	12.2			11.5	12.0
									10.1					

(3) Series III, Run 3, Spectrum I, z = -122 cm

No.	η_+	η_-	ℓ_+	ℓ_-	H	T	Hot film u_+	Hot film u_-	Hot film w_+	Hot film w_-
1	22.9	31.1	1.74	1.78	54.0	3.52	30.5	44.2	14.0	22.0
2	51.8	42.7	1.36	1.54	94.5	2.90	55.8	62.2	38.1	46.9
3	36.3	11.6	1.22	1.08	47.9	2.30	37.2	10.1	39.9	13.1
4	6.7	13.1	2.25	1.50	19.8	3.75	4.3	17.1	7.9	6.1
5	29.6	29.6	1.41	1.59	59.1	3.00	31.1	43.6	18.0	29.0
6	26.2	16.5	1.74	1.22	42.7	2.96	25.3	17.1	25.9	14.9
7	19.8	13.1	0.94	0.98	32.9	1.92	10.1	15.2	14.0	9.1
8	24.7	19.8	2.02	1.22	44.5	3.24	22.9	29.0	6.1	18.0
9	14.6	1.5	0.84	0.42	16.2	1.26	14.3	6.7	15.9	6.1
10	19.8	13.1	1.55	2.49	32.9	4.04	21.3	11.9	6.1	11.9
11	68.9	44.2	0.94	1.92	113.1	2.86	49.1	57.6	24.1	42.1
12	64.0	37.8	1.41	1.55	101.8	2.96	56.7	49.7	53.0	46.9
13	16.5	14.6	2.30	2.02	31.1	4.32	17.1	23.2	24.1	10.1
14	18.0	16.5	1.78	1.50	34.4	3.28	20.4	29.0	14.0	13.1
15	18.0	10.4	1.41	0.80	28.4	2.21	22.0	11.3	17.1	11.9
16	32.9	39.3	0.94	1.22	72.2	2.16	11.0	43.0	11.9	29.9
17	60.7	39.3	1.22	1.69	100.0	2.91	54.3	55.5	52.1	43.9
18	31.1	32.9	1.64	1.64	64.1	3.28	44.8	47.6	36.0	25.0
19	42.7	7.6	1.03	2.02	50.3	3.05	40.5	10.7	39.0	7.9
20	19.8	19.8	1.13	1.17	39.6	2.30	21.3	23.8	13.1	18.0
21	36.3	19.8	1.27	1.50	56.1	2.77	32.9	25.0	32.0	18.9
22	14.6	29.6	2.72	1.69	44.2	4.41	9.5	31.1	14.0	14.0
23	55.8	22.9	1.08	1.59	78.6	2.67	38.1	21.0	36.9	27.1
24	3.4	2.4	0.84	0.56	5.8	1.50	2.4	3.4	10.1	—
25	8.8	5.5	0.98	0.61	14.3	1.59	—	—	—	—
26	10.1	20.1	1.03	1.03	30.2	2.06	10.1	27.7	7.0	11.9
27	32.9	13.1	0.89	0.75	46.0	1.64	23.8	9.1	22.0	11.0
28	26.2	32.9	1.17	1.41	59.1	2.58	20.4	35.1	18.0	20.1
29	49.4	29.6	1.41	2.16	78.9	3.57	49.1	45.1	39.9	32.9
30	62.5	42.7	1.45	1.64	105.2	3.09	50.0	55.5	18.0	40.8
31	22.9	29.6	2.35	1.78	52.4	4.13	23.8	45.7	32.0	11.0
32	46.0	36.3	1.27	1.45	82.3	2.72	48.2	53.6	39.0	39.0
33	24.1	18.0	1.45	1.69	42.1	3.14	28.0	16.5	36.0	13.1
34	14.6	6.7	1.22	0.98	21.3	2.20	12.8	—	11.9	7.0
35	5.8	22.9	0.84	1.41	28.7	2.25	—	31.7	9.1	17.1
36	49.3	41.2	1.13	1.50	90.5	2.63	52.4	62.2	36.9	39.9
37	29.9	10.4	1.22	1.50	40.2	2.72	36.6	9.1	32.0	10.1
38	4.9	9.8	0.56	1.13	14.6	1.69	—	9.1	4.9	—
39	19.8	22.9	1.41	1.03	12.2	2.44	24.7	29.9	11.9	17.1
40	31.1	19.8	0.94	0.94	50.9	1.88	21.3	14.0	20.1	15.9
41	34.4	33.8	1.13	1.31	68.3	2.44	26.2	43.0	27.7	32.0
42	16.5	3.4	1.22	0.52	19.8	1.74	20.4	—	27.7	—
43	13.1	32.9	0.94	1.27	46.0	2.21	10.1	36.3	7.9	18.0
44	46.0	29.6	1.03	1.36	75.6	2.39	44.2	45.1	40.8	32.9
45	36.3	23.8	1.13	1.27	60.1	2.40	44.2	33.8	36.0	28.0
46	20.1	26.2	1.59	2.72	46.3	4.31	24.7	37.2	25 .0	9.1
47	67.4	47.6	1.03	1.78	114.9	2.81	57.61	70.1	39.9	47.9
48	46.6	31.1	1.31	1.64	77.7	2.95	57.6	49.1	57.9	32.9
49	26.2	18.9	1.45	1.88	45.1	3.33	31.4	20.4	35.1	17.1
50	18.9	16.5	1.41	1.22	35.4	2.63	22.9	11.9	15.9	13.1

(3) Series III, Run 3, Spectrum I, z = -122 cm (continued)

No.	η_+	η_-	ζ_+	ζ_-	H	T	Hot film u_+	Hot film u_-	Hot film w_+	Hot film w_-
51	5.8	4.0	1.13	0.66	9.8	1.79	4.3	1.2	10.1	4.0
52	20.7	36.3	1.31	1.55	57.0	2.86	24.7	50.3	7.0	22.9
53	55.8	22.9	1.13	2.25	78.6	3.38	48.2	21.0	46.0	25.9
54	26.2	34.4	1.36	1.22	60.7	2.58	40.5	49.1	10.1	32.9
55	32.9	31.4	1.03	1.22	50.9	2.25	32.3	15.9	38.1	20.1
56	19.8	19.8	1.17	1.22	50.9	2.25	32.3	15.9	22.0	20.1
57	32.9	26.2	1.27	1.31	59.1	2.58	46.6	45.7	22.0	29.0
58	41.2	41.2	1.41	1.88	82.3	3.29	50.9	66.1	36.0	36.9
59									42.1	

(4) Series III, Run 4, Spectrum II, z = -122 cm

No.	η_+	η_-	ζ_+	ζ_-	H	T	Hot film u_+	Hot film u_-	Hot film w_+	Hot film w_-
1	8.5	13.1	1.27	1.50	21.6	2.77	17.7	14.0	10.0	11.0
2	9.8	16.5	2.95	1.31	26.2	4.26	15.2	18.6	13.1	11.0
3	29.6	29.6	1.27	1.27	59.1	2.54	35.7	37.5	22.0	27.1
4	32.9	23.8	1.08	1.08	56.7	2.16	29.0	27.7	29.9	25.9
5	21.3	12.5	1.13	1.97	33.8	3.10	17.1	13.7	24.1	14.0
6	7.0	7.3	1.27	1.55	14.3	2.82	6.7	10.1	7.9	7.0
7	3.4	8.2	0.56	1.31	11.6	1.87	3.4	12.5	6.1	7.0
8	19.8	24.7	1.17	1.27	44.5	2.44	18.6	32.3	13.1	20.1
9	22.3	11.6	1.13	0.94	33.8	2.07	37.2	14.6	22.9	13.1
10	8.5	4.9	0.84	1.41	13.4	2.25	10.1	6.7	7.9	3.7
11	9.8	14.6	1.50	1.13	24.4	2.63	13.4	15.9	7.0	11.9
12	13.1	12.8	1.59	1.31	25.9	2.90	17.7	14.0	13.1	9.1
13	18.0	14.6	1.13	0.70	32.6	1.83	20.4	10.1	13.1	11.0
14	28.0	23.8	0.84	1.41	51.8	2.25	17.7	29.6	11.0	18.9
15	36.3	26.8	1.22	1.50	63.1	2.72	42.4	31.7	29.0	27.1
16	19.8	14.6	1.55	1.59	34.4	3.14	24.7	22.0	18.9	13.1
17	32.9	19.8	1.22	1.59	52.7	2.81	32.3	29.9	15.9	22.0
18	26.2	6.7	1.36	1.27	32.9	2.63	22.0	4.0	20.1	9.1
19	5.5	28.0	0.56	1.31	33.5	1.87	2.4	41.8	0.9	10.1
20	55.2	36.3	1.22	1.78	91.4	3.00	51.8	58.2	39.9	36.0
21	39.3	29.6	1.27	1.64	68.9	2.91	41.5	39.6	39.0	27.1
22	39.9	24.7	1.27	1.41	64.6	2.68	36.6	33.8	38.1	28.0
23	21.3	24.7	1.69	1.13	46.0	2.82	22.9	22.6	24.1	18.9
24	9.8	1.5	0.70	0.61	11.3	0.31	7.6	4.0	11.9	—
25	13.1	9.8	1.41	0.94	22.9	2.35	15.2	7.9	6.1	9.1
26	15.9	24.7	1.03	1.22	68.6	2.25	15.2	29.0	11.0	15.9
27	46.0	25.6	1.13	1.69	86.0	2.82	48.2	43.0	32.0	29.9
28	21.3	10.4	1.27	2.06	101.5	3.33	34.8	13.1	24.1	11.9
29	19.8	19.8	0.98	1.17	65.5	2.15	26.2	16.5	10.1	15.9
30	12.8	22.9	1.48	1.08	77.1	2.53	15.2	17.1	13.1	15.9
31	19.8	3.4	1.03	0.80	55.8	1.83	11.9	3.4	14.9	7.9
32	3.4	11.0	0.75	1.17	58.5	1.92	5.8	12.5	2.1	6.1
33	10.1	7.6	0.89	0.84	52.7	1.73	6.7	—	6.1	—

(4) Series III, Run 4, Spectrum II, z = -122 cm (continued)

No.	η_+	η_-	ℓ_+	ℓ_-	H	T	Hot film u_+	Hot film u_-	Hot film w_+	Hot film w_-
34	8.2	26.2	1.41	1.31	34.4	2.54	8.5	30.5	7.0	13.1
35	39.3	6.7	1.08	0.89	46.0	1.97	22.9	5.2	28.0	11.9
36	3.4	14.6	0.33	1.45	14.9	1.78	—	17.1	—	—
37	13.1	23.8	2.25	1.88	36.9	4.13	17.7	29.9	9.1	—
38	65.5	18.0	1.03	1.97	83.5	3.00	49.1	28.4	29.9	22.9
39	13.1	19.8	2.30	1.50	32.9	3.80	20.4	22.6	7.9	10.1
40	22.9	3.4	1.13	0.61	26.2	1.74	22.9	—	20.1	—
41	6.7	16.5	0.61	1.03	23.2	1.64	—	15.9	—	—
42	14.6	13.4	1.41	1.17	28.0	2.58	20.4	14.0	15.9	14.0
43	13.1	8.5	1.17	1.27	21.6	2.44	11.9	7.9	13.1	11.0
44	1.5	4.9	1.31	0.84	6.4	2.15	—	—	—	—
45	32.9	24.7	0.80	1.17	57.6	1.97	22.0	29.0	—	20.1
46	14.6	18.9	1.50	1.17	33.5	2.67	17.7	18.0	15.9	14.9
47	21.3	13.1	0.98	1.17	34.4	2.15	15.2	16.5	18.0	14.9
48	6.7	6.7	1.31	1.03	13.4	2.34	12.8	9.1	10.1	6.1
49	18.0	19.8	0.84	0.94	37.8	1.78	6.7	16.5	6.1	14.0
50	22.9	19.8	1.41	1.22	42.7	2.63	23.8	26.5	18.9	18.0
51	14.6	24.1	2.11	1.36	38.7	3.47	20.4	27.1	16.2	14.0
52	28.0	36.6	2.06	1.27	64.6	3.33	29.0	49.7	14.0	32.0
53	41.2	13.1	1.08	1.31	54.3	2.39	34.8	13.1	39.9	18.0
54	4.9	8.2	1.97	0.84	13.1	2.81	4.3	4.6	7.9	4.9
55	14.6	17.4	1.22	1.22	32.0	2.44	12.8	16.5	10.1	14.0
56	16.4	21.3	1.69	1.59	37.8	3.28	20.4	33.8	15.9	14.0
57	41.2	22.9	1.13	1.42	64.0	2.54	40.5	33.2	27.1	28.0
58	34.4	29.6	1.31	1.17	64.0	2.48	33.8	31.7	28.0	32.9
59	55.8	29.9	1.27	1.69	85.6	2.96	46.6	38.4	43.9	35.1
60	18.9	11.6	1.50	1.88	30.5	3.39	19.6	11.3	22.0	11.9
61	15.9	19.8	1.41	1.22	35.7	2.63	14.3	18.0	7.0	14.9
62	29.6	22.9	0.94	1.13	52.4	2.07	20.4	21.0	18.9	21.0
63	16.5	7.6	0.94	1.03	24.1	1.97	10.1	7.3	18.0	10.1
64									4.9	